United States
Department of
Agriculture

Forest Service

**Intermountain
Research Station**

Research Paper
INT-407

July 1989

Characteristics of Long Vertical DC Arc Discharges

Don J. Latham

THE AUTHOR

DON J. LATHAM received his bachelor's degree in physics from Pomona College in 1960, and his master's in 1964 and Ph. D. in 1967, both in earth science, from the New Mexico Institute of Mining and Technology. From 1968 to 1976 he taught and did research in atmospheric electricity in the Rosenstiel School of Marine and Atmospheric Science, University of Miami. In 1976 he joined the Intermountain Research Station's Intermountain Fire Sciences Laboratory (formerly Northern Forest Fire Laboratory), in Missoula, MT, as a research meterologist/physicist.

RESEARCH SUMMARY

Vertical electric arc discharges of varying lengths to a maximum of 10 cm were drawn between carbon electrodes. The arcs were powered by a bank of 40 series-connected lead-acid batteries, with a Silicon-controlled-rectifier switch for accurate timing. Initiation of the arc was accomplished by three methods, two using tungsten wire and one a moving carbon electrode. Current was limited by a series resistance made of carbon rods.

Current in the circuit and voltage across the arc were measured for several values of current and electrode spacing. The measurements showed that the voltage drop across the arc is independent of current and dependent only on electrode spacing, and did not depend on how the arc was initiated. The current in the arc, on the other hand, was independent of the arc spacing and initiation method and depended only on the source resistance and source voltage, or, equivalently, on the current in the circuit if the arc was replaced with zero resistance.

Observations were made of some arcs with a 1,000-frame-per-second video system. The results showed the presence in all arcs of a cathode and an anode jet. The jets did not meet in an organized fashion, but behaved rather as two streams of water might. The anode jet wandered around the cathode jet, which was very nearly stationary. There seems to be a balance between minimum resistance, that is a hot gas column in a straight line between the electrodes, and the instability of two hot gas jets meeting colinearly in opposite directions. Due to time and data constraints, this system was analyzed in qualitative terms.

CONTENTS

Intermountain Research Station
324 25th Street
Ogden, UT 84401

Characteristics of Long Vertical DC Arc Discharges

Don J. Latham

INTRODUCTION

This paper contains observations of the operating characteristics and behavior of a vertical dc arc ignition source. The construction of the source is given in Latham (1987). The arc system was made to obtain ignition probabilities for wildland fine fuels subjected to electrically generated ignition sources such as lightning or downed powerlines. A simplified diagram of the system appears as figure 1.

The arc is generated by switching a 500-v (nominal) source in series with a resistance across a 9-cm (nominal) gap between two carbon rod electrodes. The gap is initially shorted by a 0.1-mm-diameter tungsten wire. The wire, upon initiation of current flow, heats and then burns, creating an ionized medium in which the arc forms. At the end of the desired time interval, the voltage source is interrupted, leaving a hot gas channel that decays to ambient temperature through radiation and diffusion (Latham 1986). In use, typical fuels are arranged around the wire and are then heated by the arc. Arc current and duration, together with fuel state parameters, were varied to obtain ignition probabilities. A later adaptation of the device used a moving electrode to strike the arc, but the basic testing procedure remained the same.

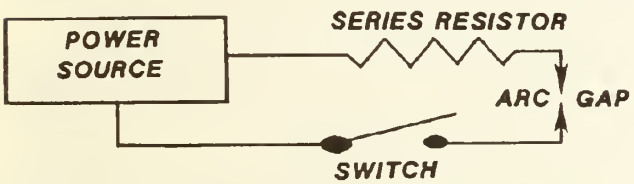

Figure 1—A simplified arc electrical circuit diagram.

Figure 2 is an example of an actual record of current and voltage traces for an arc generated by the system. Portions of the arc time behavior are labeled in the caption. The initial current onset is called the starting transient (1). Following that is the wire heating and ionizing portion (2), then the arc striking time (3), the main arc, or arc proper (4), and the stopping transient (5).

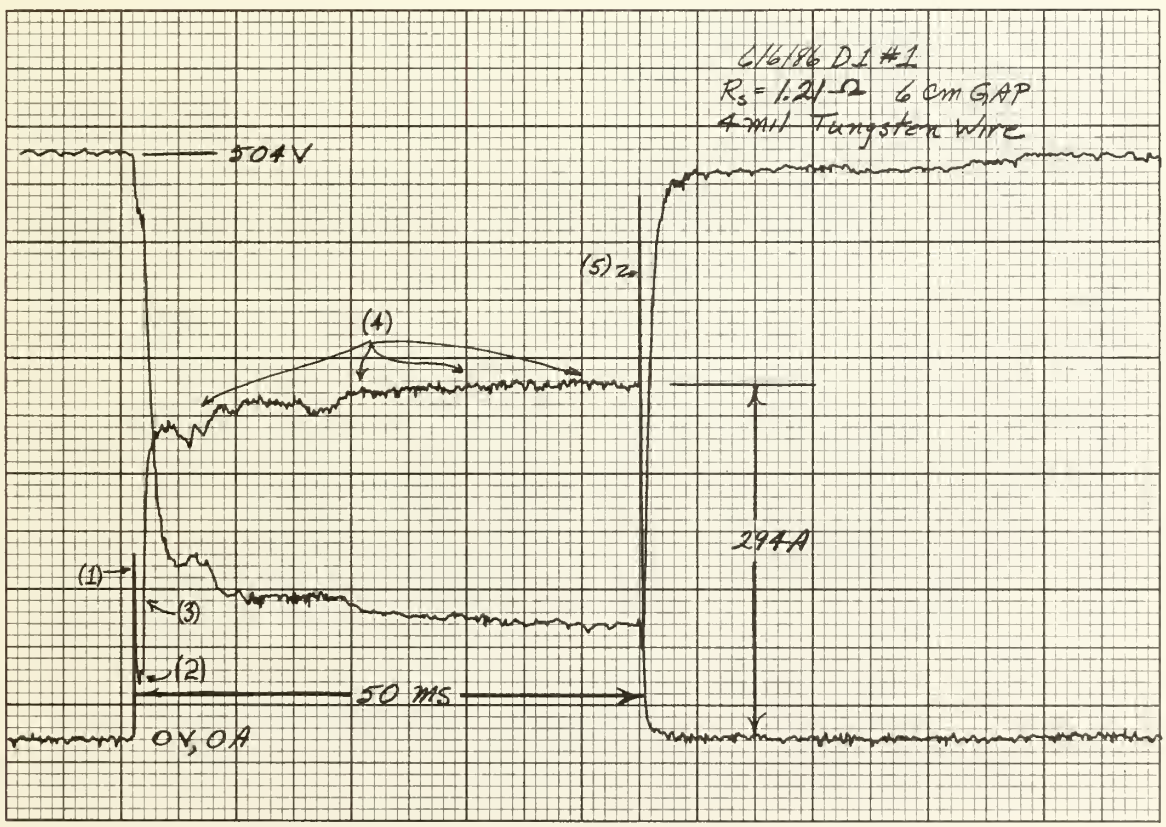

Figure 2—Current and voltage behavior with time for a typical arc in this study. Arc behavior segments are indicated: (1) starting transient, (2) wire heating and ionizing, (3) arc striking, (4) main arc duration, and (5) stopping transient.

The measurement of the gross characteristics of the arc, that is, the way the current in the arc and the voltage drop across it vary with gap length and source conductance was the main emphasis of the phase of the study reported here. We found that the voltage drop increased with gap length in a regular way. For a fixed gap length, and increasing short-circuit current, the arc current increased. The arc voltage drop, in other words, depends almost entirely on the arc length, and the arc current almost entirely on the source short-circuit current, as the model (Latham 1986) predicts.

Arc behavior was recorded with a 1000-image-per-second video camera. The flow patterns in the arc seem to be dominated by a jet from the anode and one from the cathode. The meeting of these two jets is not stable, yet the arc, considered as an electrical circuit element, is stable, as the current measurements show clearly.

The results of these investigations did show that the arc was suitable for the purpose of obtaining probability of fuel ignition.

INSTRUMENTATION

Construction details of the arc electric circuit measuring devices are given in Latham (1987). Briefly, the current in the circuit is measured with a Hall effect device, the voltage across the arc gap or series resistor with a calibrated resistive divider and isolation amplifier, and arc luminosity with an Si detector. The current and voltage devices are calibrated to 1 percent, but due to well-known difficulties with radiation measurements, the luminosity measurement is relative from event to event, and serves as a qualitative indicator only. No luminosity was evident in the source characteristic observations. Data were recorded on a Nicolet two-channel sampling oscilloscope with 12-bit precision and floppy disk storage. This recording technique enabled easy data recovery and precise measurement of timing and amplitude. Except for possibly missing very fast transients, errors due to data storage and retrieval can be considered negligible. A typical measurement taken with a shorted arc is shown in figure 3.

Figure 4 shows the result of an analysis of 53 cases in which the conductance was varied and the short-circuit current measured. Because the voltage source is made up of lead-acid batteries, the source voltage is a function of the current drawn, as the figure shows. The variability apparent in the figure is due to the large number of electrical contacts in the system, and cannot be avoided. Part of the variability is also due to the differing state of charge and temperature of the batteries. These factors necessitate measurement of voltage across the arc and also the current in the arc circuit during operation.

Discussion of the calibration of the current sensor will also provide insight as to the effect of resistance temperature variation and source variability. The calibration procedure was as follows: the arc gap was shorted, as previously described. The isolated voltmeter, separately

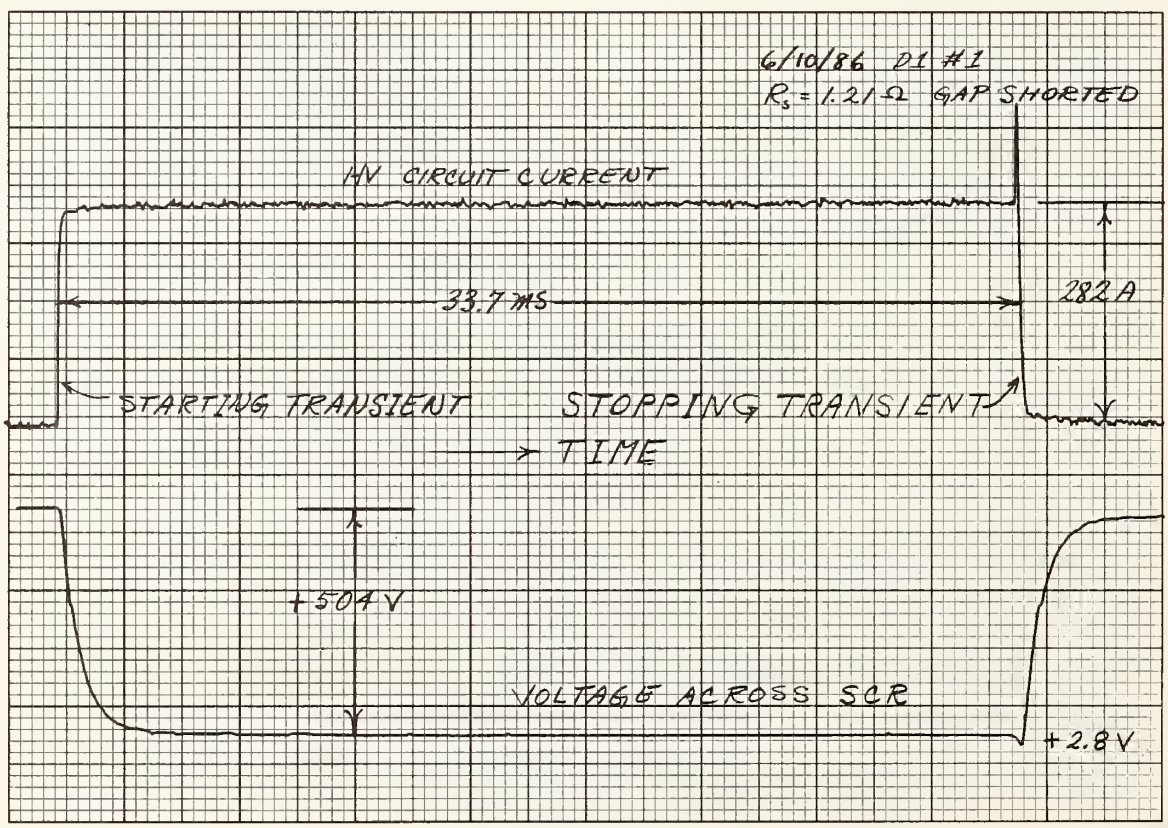

Figure 3—Current and voltage behavior for the system with the arc gap electrically shorted.

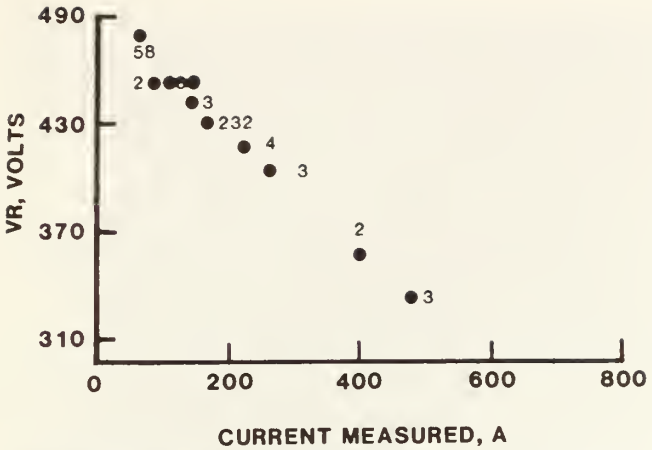

Unweighted least squares linear regression of VR

Predictor variables	Coefficient	Std error	Student's T	P
Constant	486.29	1.2896	377.08	0.0000
Curmeas	–3.0232E-01	5.7009E-03	–53.03	.0000

Cases included	53	Missing cases	0
Degrees of freedom	51		
Overall F	2.812E+03	P value	0.0000
Adjusted R^2	0.9818		
R^2	0.9822		
Resid. mean square	27.87		

Figure 4—A plot of voltage drop across the series resistor (in volts) vs. measured circuit current (in amperes). The results of a linear regression analysis are included.

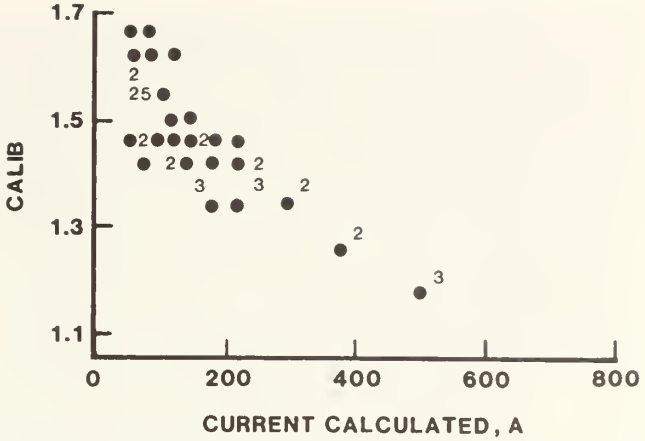

Unweighted least squares linear regression of calib

Predictor variables	Coefficient	Std error	Student's T	P
Constant	1.5886	1.3024E-02	121.97	0.0000
Curcalc	–7.6517E-04	5.7244E-05	–13.37	0.0000

Cases included	53	Missing cases	0
Degrees of freedom	51		
Overall F	178.7	P value	0.0000
Adjusted R^2	0.7736		
R^2	0.7779		
Resid. mean square	2.911E-03		

Figure 5—Magnetic field device calibration factor (dimensionless) vs. calculated current (in amperes) in the arc circuit. A linear regression analysis is included.

calibrated against a digital voltmeter ($4^1/2$ digits precision) was connected across the carbon rod resistor. The cold resistance of the rod was measured with a Wheatstone bridge (5-digit accuracy) and the circuit energized. The voltage and current were measured with the digitizing oscilloscope (12-bit precision). This procedure was carried out with varying cold resistances, with 53 data points taken.

The calibration factor for the current device is obtained by dividing the measured millivolt value into a current calculated from the measured voltage and cold resistance. The results are given in figure 5. If the resistance of the rod resistor were constant, the value of this calibration ratio would show a random scatter about some mean value. Instead, we found a steady decrease in the calibration value with increasing current. This decrease is due to the resistor having a value different from the cold value. As the current increases, the resistance decreases. Systematic variations in the calibration factor CALIB of figure 5 are due only to changes in the resistance produced by heating. The calibration factor is the zero-current value, or the constant in a linear regression (fig. 5). This calibration value is 1.59 a/mv.

SOURCE CHARACTERISTICS

Source characteristics, the current carrying capacity of the voltage and series resistance of figure 1, and the behavior of the SCR switching circuit were obtained by measuring current and voltage with a shorted gap and varying the source resistance. Time details of typical current and voltage measurements for the shorted gap are shown in figures 3 and 6 through 9. Figure 3 contains some nomenclature information as well. Note the portions of the records labeled starting transient and stopping transient; details of these are given in figures 7, 8, and 9. Also shown clearly in figure 3 is the poor time response of the voltage isolation amplifier, causing problems with the interpretation of fast-occurring details of the source and arc observations.

There is nothing remarkable about the current structure with respect to time in the shorted gap case. There is a small rise in the current during the short pulse of figure 3, a rise more evident in the longer pulse of figure 6. This current increase is accounted for by the temperature rise in the series resistor carbon rods. This same rise is part of the reason for the higher current in figure 4 as opposed to that of figure 3. Variation in the current under supposedly identical conditions is due in part to the presence, for

safety reasons, of 22 contacts in the battery power supply. At the high currents in the circuit, a small resistance change can mean a large current change. In addition, the batteries in the power supply have the characteristic that voltage decreases as current drain increases.

Figure 7 shows a current record for the very beginning of the starting transient. The current rate of rise in this measurement is several orders of magnitude higher than the rate of current rise limit for the silicon controlled rectifier (SCR) switch. This current may be due to charging of the internal capacitance of the SCR. Note that on this timescale, the gate trigger pulse (not shown) is still on its risetime slope and may not have completely turned on the switch. The instrumentation unfortunately prevents a look at the voltage behavior on this time scale.

The actual turn-on pulse of the SCR switch is displayed in figure 8. The rate of rise here is about 1.4 a/μs, well within the design specification of the switch. This slow rise is due to the inductance of the leads from the battery power supply to the experimental apparatus. The duration of the current rise, on the order of tens of milliseconds, is consonant with the design specifications of the SCR. The turn-on pulse holds no surprises.

Turn-off of the arc supply voltage (fig. 9) is accomplished by a process called decommutation, that is, a current pulse from a capacitor counters the current in the SCR switch and, in the absence of a trigger voltage on the switch gate, stops conduction. There is again an extremely rapid high current pulse and a momentary increase in the current flow as the supply tries to discharge the decommutating capacitor. Note that in figures 3 and 6, only one of the high-current, very short pulses has been captured—the stopping transient in figure 3. This is due to the sampling interval in the recording oscilloscope.

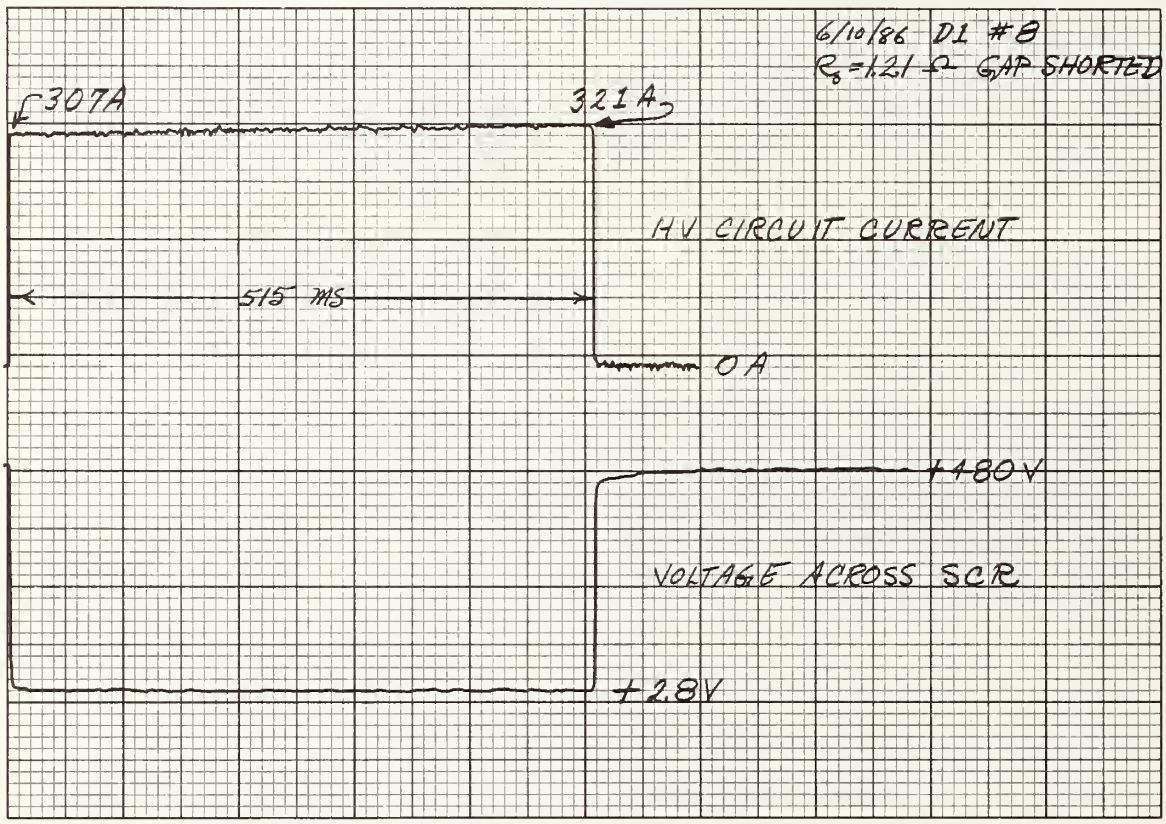

Figure 6—Measurements of the time behavior of circuit current and the voltage across the SCR switch. The effect of heating of the series resistor is apparent.

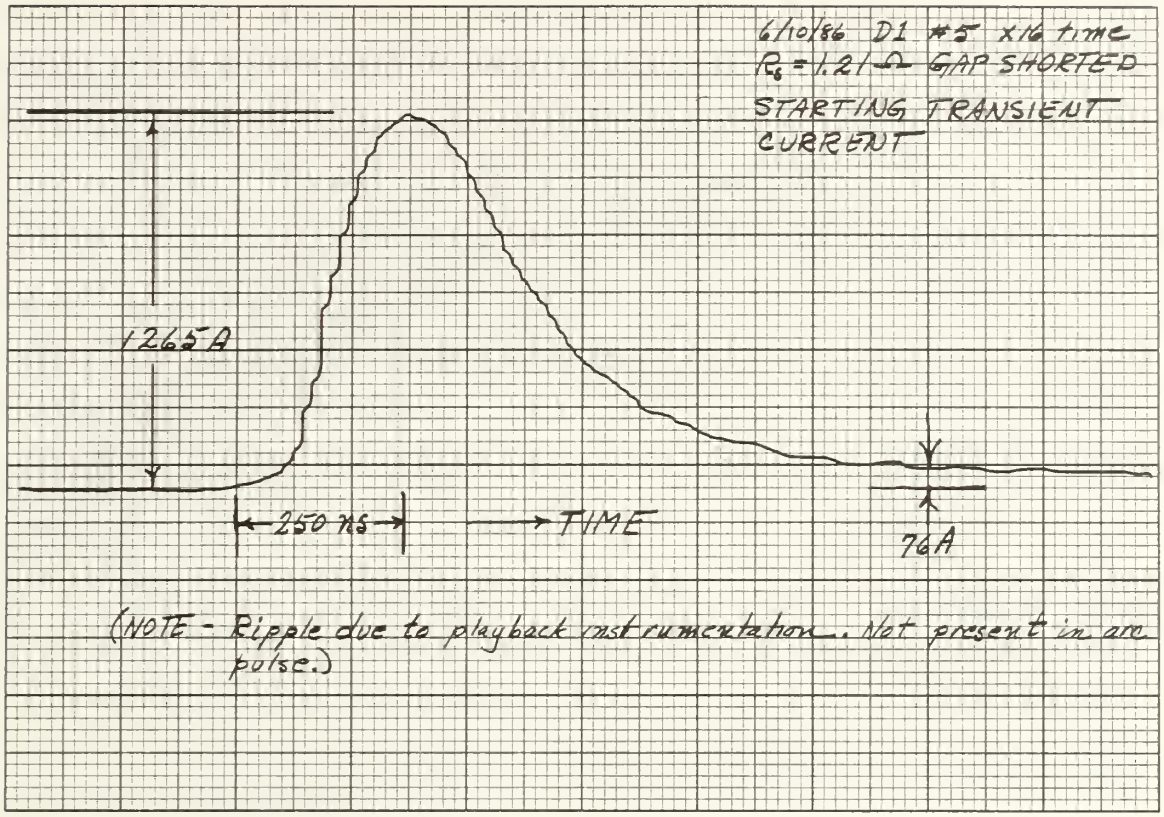

Figure 7—Circuit current behavior with time for the turn-on pulse. Note the large peak current.

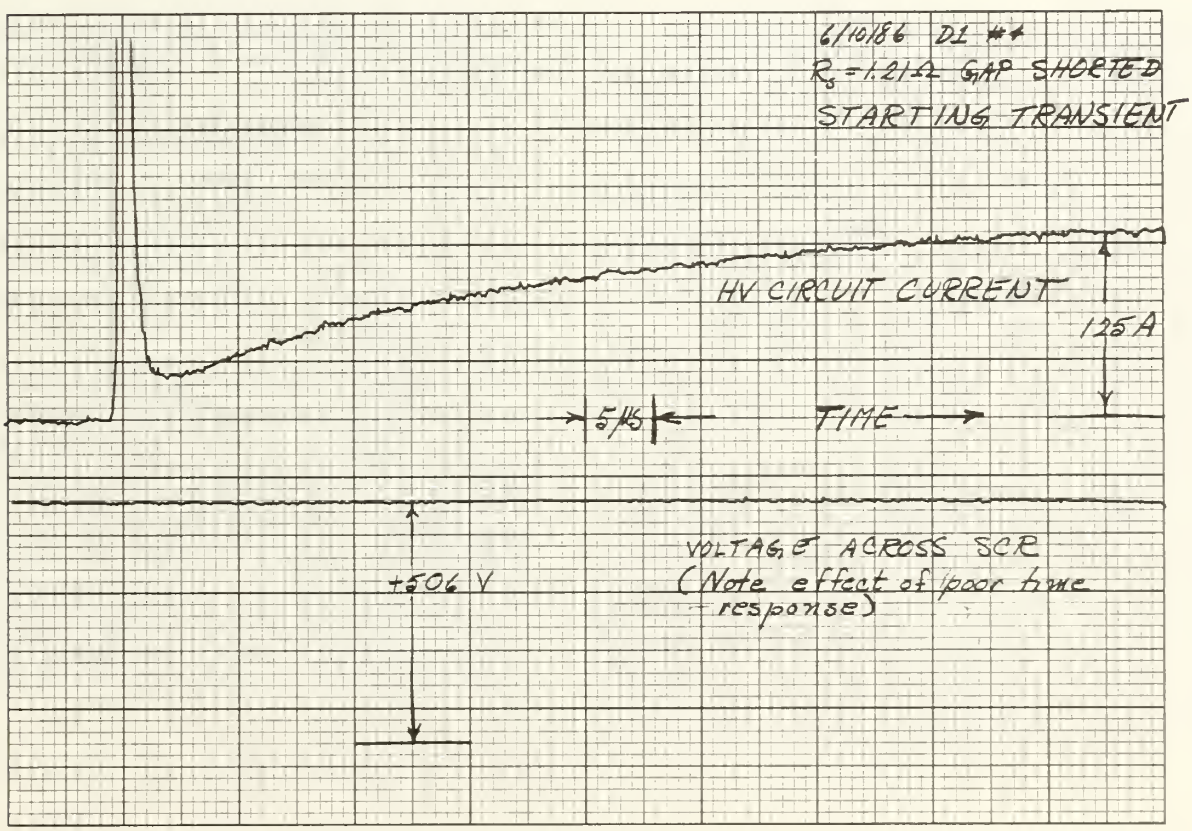

Figure 8—Circuit current behavior with time for the initial 50 microseconds of the turn-on.

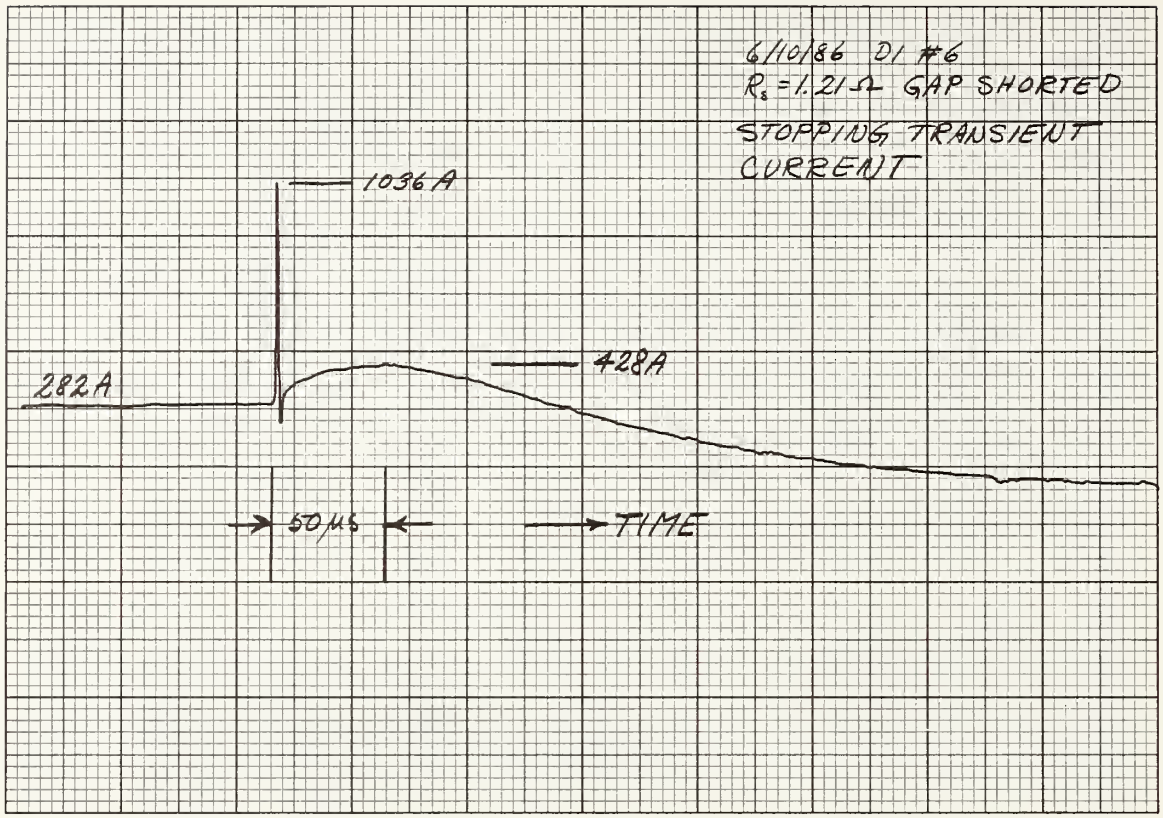

Figure 9—Circuit current behavior for the stopping transient.

GROSS ARC CHARACTERISTICS

Arc behavior is reported in two parts: (1) the current and voltage drop as dependent variables taken as averages over a portion of the arc duration, and (2) the short-term details of current, voltage, and arc structure, the latter as recorded by high-speed video. Current and voltage are read directly from the storage oscilloscope. The period during the arc when the current and voltage are taken is somewhat subjective. The arc must be stable, and sufficient time elapsed from arc initiation for the voltage amplifier to have settled to a steady value. In the traces of figure 2, for example, the current and voltage values would be taken over the last 30 ms of the arc duration.

The data shown in the remainder of the paper were taken using three different geometrical arrangements for the exploding wire ignition system. The first, used until the high-speed video data were obtained, is schematically presented in figure 10. The wire was drawn taut across the edges of the cylindrical electrodes. The belief that the arc would form vertically between the electrodes proved to be incorrect. The slow-motion visual data led to the more concentric ignition arrangement of figure 11. This coaxial structure seems to provide a more stable arc than the simple one of figure 10, although we do not have visual proof. These two methods will be referred to hereafter as "side strike" and "center strike," respectively.

A third striking method (fig. 12) was added to the system to ease ignition studies in peat, punky wood, and short-needled tree duff. The arc apparatus was modified so that an 8-mm-diameter rod could be placed in contact with the anode, the current switched on, and the cathode rod drawn down through the fuel bed. Measurements indicated no significant difference in gross arc behavior. There is, of course, a significant difference in the short-term arc behavior.

The independent electrical variables for the arc experiment are those that are controlled or are controllable. For the arc experiment, these were the gap length (that is, the length between anode and cathode electrodes), the series resistance in the circuit, and the arc duration. We could have controlled the source voltage as well, but would have needed more batteries for this control to be meaningful. The length of the arc is not, as we will show, the same as the gap distance. The dependent electrical variables in our experiment are defined as the current in the arc circuit and the total voltage drop across the circuit.

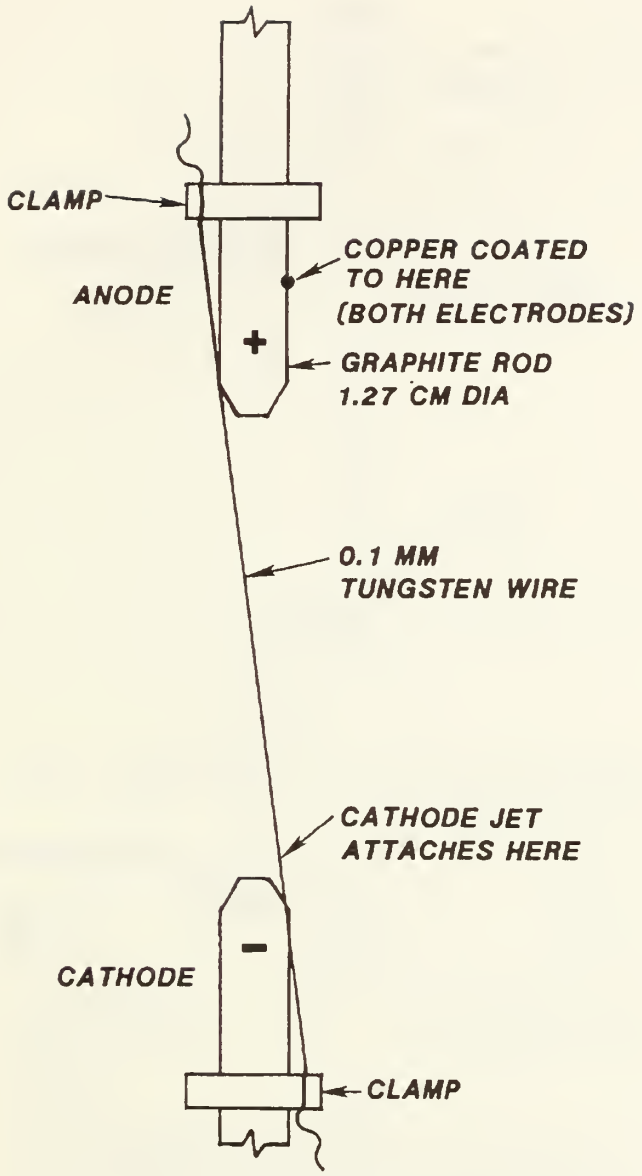

Figure 10—Exploding wire arrangement for the side strike method.

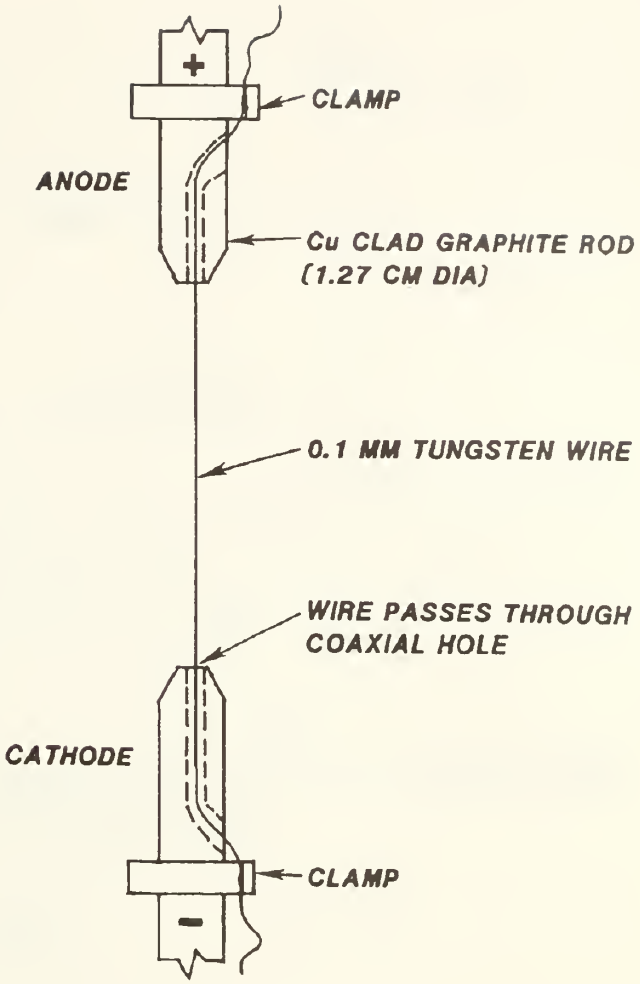

Figure 11—Exploding wire arrangement for the center strike method.

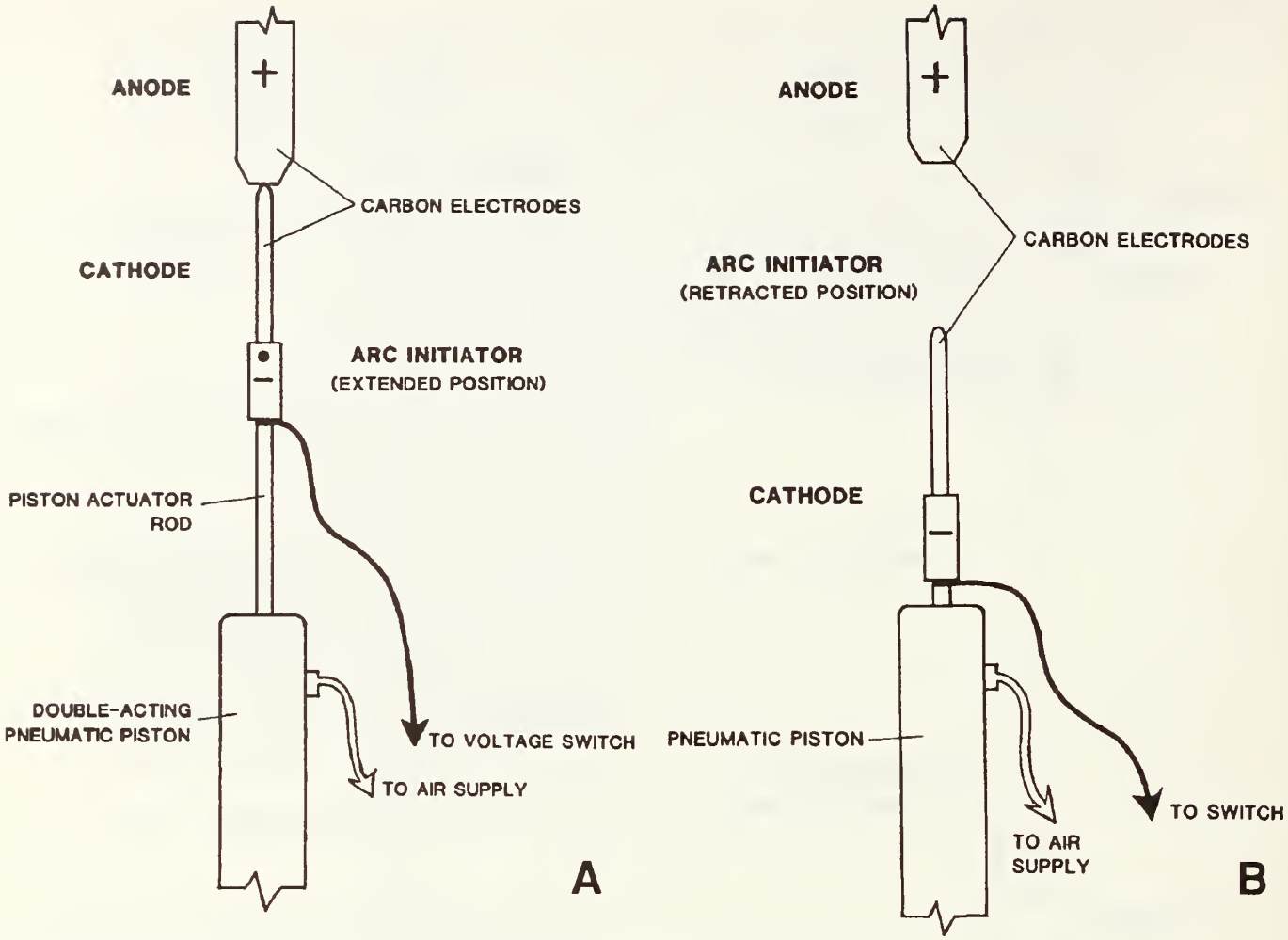

Figure 12—(a) Pneumatic arc initiator in the extended position; (b) the same in the retracted position.

The usual way of reporting arc behavior (see, for example, Von Engel 1965) is by a plot of the arc characteristic. This is a plot of the current in the arc circuit vs. the voltage drop across the arc. Some results from our observations are plotted in this way in figure 13. This figure demonstrates that the voltage drop across the gap is independent, or nearly so, of the current. This was pointed out in Latham (1986) to be a consequence of the free boundary of the arc column, and is not the case for arcs constrained by boundaries or flow control. The scatter in the data points will be explained in the more detailed analysis presented later. The independence of voltage and current was also found, but not explained, by King (1961) for free vertical arcs with about the same gap distances. King also noted a large scatter in his arc data, which he reports as nearly a factor of 2, as did Strom (1946) for very long arcs driven by a 60-Hz source. Strachan and Barrault (1975) report independence of axial electric field from peak current.

Dependence of arc voltage and current for side and center strike as functions of arc gap (GAP) and source conductance (COND) is given in tables 1 through 4 and figures 14 and 15. The figures are based on the analyses in the tables. Data points are not shown on the figures for clarity. As suggested by figure 13, the voltage is very nearly independent of the conductivity, and the current is very nearly independent of the arc gap. Admittedly, we have forced a linear dependence through analysis. The fit of the data, however, is good in case of the voltage (tables 1 and 3), which should be gap-dependent (Latham 1986), and excellent in the case of current (tables 2 and 4), as expressed by the appropriate r^2 values.

Figure 14, voltage across arc vs. the arc gap with conductance as a parameter, graphically demonstrates the near independence of the voltage from conductance. The figure is generated from tables 1 and 2, and gives the results of a linear regression. Linearity is a good assumption for this combination of variables, except for gaps less than 1 cm or so, where cathode and anode flows merge and completely dominate the behavior (see, for example, von Engel [1965], fig. 132, and Sommerville [1959], fig. 6).

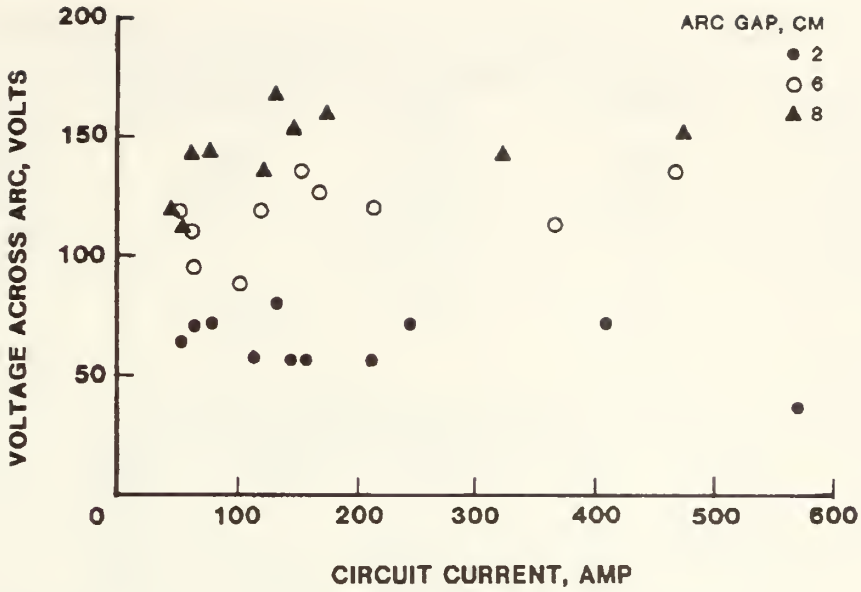

Figure 13—Voltage across the arc as a function of circuit current for three arc gap values.

Table 1—Linear regression for voltage as a function of gap (cm) and source conductance (s) for the side-strike method

	Unweighted least squares linear regression of voltage			
Predictor variables	**Coefficient**	**Std error**	**Student's T**	**P**
Constant	47.881	4.2469	11.27	0.0000
Gap	8.5905	6.7963E–01	12.64	.0000
CS	–3.7067	5.1161	–0.72	.4740

Cases included	35	Missing cases	0
Degrees of freedom	32		
Overall F	95.06	P value	0.0000
Adjusted R^2	.8469		
R^2	.8559		
Resid. mean square	94.30		

	Stepwise analysis of variance of voltage					
Source	**Individual SS**	**Cum. DF**	**Cumulative SS**	**Cumulative MS**	**Adjusted R^2**	**Mallow's CP**
Constant	3.5829E+05					
Gap	1.7878E+04	1	1.7878E+04	1.7878E+04	0.8491	1.5
CS	49.500	2	1.7928E+04	8963.9	.8469	3.0
Residual	3017.4	34	2.0945E+04	616.04		

Cases included	35	Missing cases	0
Degrees of freedom	32		
Overall F	95.06	P value	0.0000
Adjusted R^2	.8469		
R^2	.8559		
Resid. mean square	94.30		

Table 2—Linear regression for voltage as a function of gap (cm) and source conductance (s) for the center-strike method

	Unweighted least squares linear regression of voltage			
Predictor variables	**Coefficient**	**Std error**	**Student's T**	**P**
Constant	45.340	4.5524	9.96	0.0000
Gap	10.985	5.8708E–01	18.71	.0000
CS	9.9032	3.8173	2.59	.0106

Cases included	101	Missing cases	0
Degrees of freedom	98		
Overall F	179.2	P value	0.0000
Adjusted R^2	.7809		
R^2	.7853		
Resid. mean square	294.6		

	Stepwise analysis of variance of voltage					
Source	**Individual SS**	**Cum. DF**	**Cumulative SS**	**Cumulative MS**	**Adjusted R^2**	**Mallow's CP**
Constant	1.4824E+06					
Gap	1.0362E+05	1	1.0362E+05	1.0362E+05	0.7683	7.7
CS	1982.7	2	1.0560E+05	5.2802E+04	.7809	3.0
Residual	2.8870E+04	100	1.3447E+05	1344.7		

Cases included	101	Missing cases	0
Degrees of freedom	98		
Overall F	179.2	P value	0.0000
Adjusted R^2	.7809		
R^2	.7853		
Resid. mean square	294.6		

Table 3—Linear regression for current as a function of gap (cm) and source conductance (s) for the side-strike method

	Unweighted least squares linear regression of current			
Predictor variables	**Coefficient**	**Std error**	**Student's T**	**P**
Constant	33.621	3.3675	9.98	0.0000
Gap	–4.0993	5.3890E–01	–7.61	.0000
CS	320.23	4.0567	78.94	.0000

Cases included	35	Missing cases	0
Degrees of freedom	32		
Overall F	3.595E+03	P value	0.0000
Adjusted R^2	.9953		
R^2	.9956		
Resid. mean square	59.29		

	Stepwise analysis of variance of current					
Source	**Individual SS**	**Cum. DF**	**Cumulative SS**	**Cumulative MS**	**Adjusted R^2**	**Mallow's CP**
Constant	8.5301E+05					
Gap	5.6845E+04	1	5.6845E+04	5.6845E+04	0.1065	6232.3
CS	3.6943E+05	2	4.2628E+05	2.1314E+05	.9953	3.0
Residual	1897.2	34	4.2818E+05	1.2593E+04		

Cases included	35	Missing cases	0
Degrees of freedom	32		
Overall F	3.595E+03	P value	0.0000
Adjusted R^2	.9953		
R^2	.9956		
Resid. mean square	59.29		

Table 4—Linear regression for current as a function of gap (cm) and source conductance (s) for the center-strike method

Predictor variables	Unweighted least squares linear regression of current			
	Coefficient	Std error	Student's T	P
Constant	53.155	4.2888	12.39	0.0000
Gap	−5.4099	5.5308E−01	−9.78	.0000
CS	300.04	3.5962	83.43	.0000

Cases included	101	Missing cases	0
Degrees of freedom	98		
Overall F	3.516E+03	P value	0.0000
Adjusted R^2	.9860		
R^2	.9863		
Resid. mean square	261.5		

	Stepwise analysis of variance of current					
Source	Individual SS	Cum. DF	Cumulative SS	Cumulative MS	Adjusted R^2	Mallow's CP
Constant	2.9168E+06					
Gap	1.8643E+04	1	1.8643E+04	1.8643E+04	0.0000	6961.9
CS	1.8200E+06	2	1.8387E+06	9.1933E+05	.9860	3.0
Residual	2.5623E+04	100	1.8643E+06	1.8643E+04		

Cases included	101	Missing cases	0
Degrees of freedom	98		
Overall F	3.516E+03	P value	0.0000
Adjusted R^2	.9860		
R^2	.9863		
Resid. mean square	261.5		

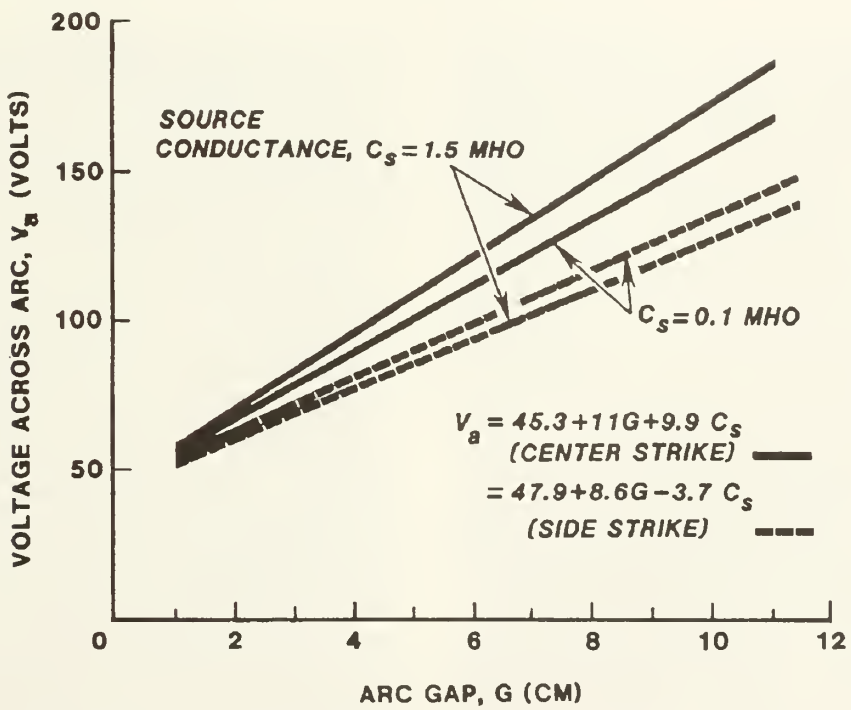

Figure 14—The voltage drop across the arc as a function of arc gap for two values of series conductance. Results of analysis of side-strike and center-strike methods are shown.

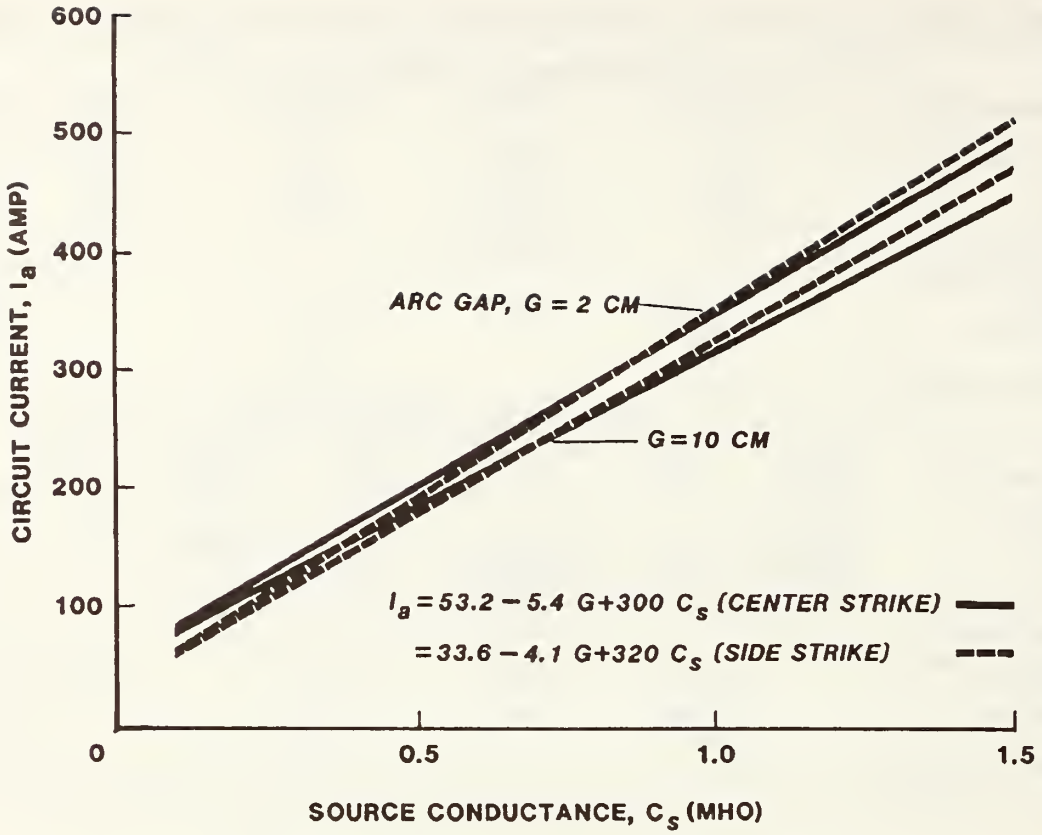

Figure 15—Circuit current presented as a function of source conductance for two arc gaps. Results of analysis of side-strike and center-strike methods are shown.

The slope of the voltage curves gives the mean electric field for arcs longer than 1 cm. If flow structure is not important, there should be little difference between side strike and center strike results. There is some difference in these figures; 11 V/cm in the center strike case and 8.6 V/cm in the side strike. This indicates that the side strike arcs may be in some way shorter than the center strike arcs, or that the structure of the anode and/or cathode columns are different. We have no way of determining the difference at present. Strom's (1946) arcs were 25-50 cm long, and had electric fields which, although showing large scatter, averaged 13 V/cm, close to our values of 8 and 11 V/cm.

The dependence of the voltage across the arc on source conductance is very small, and changes sign according to the striking method (tables 1, 2), being negative for side strike and positive for center strike (fig. 14). The statistics in the tables also show that if the arc voltage drop is related to conductance, the relationship is very weak indeed. Figure 13 demonstrates also that the current and voltage are independent from each other. The noise in the measurements on figure 13, together with the sign change in dependence, means that there is no apparent systematic relationship between voltage and current and, for our circuit, its surrogate, conductance.

The anode and cathode each has an associated voltage drop. The sum of these is the intercept of the voltage vs. gap curves in figure 14 (from tables 1 and 2). These values, 45.3 V for the center strike arcs and 47.9 V for the side strike arcs, are reasonable according to von Engel (1965) (see the figure cited above). The actual "electrode drop" is somewhat less than the intercepts given above, and is highly dependent on the electrode structure, material, and the "working gas." We did not investigate this phenomenon in this study.

Figure 15 and tables 3 and 4 summarize the relationship between current and arc gap and circuit conductance. The statistics in the tables demonstrate clearly that the possibility of systematic dependence of current on arc gap is small. The addition of the gap variable to the regression adds essentially no new information. Again, as with voltage, we must be careful to state the limitations of this analysis. Arcs shorter than 1 cm or so will not follow the equations developed here. In addition, there is the possibility that substantially longer arcs, or higher current arcs, may not either. Because there should be no current flow at zero conductance (infinite series resistance), it is certain that the linear analysis will fall apart at conductances less than 0.1 S or so, as is evident from figure 16.

That the current does depend slightly on electrode gap is apparent from figure 16. In general, as the current increases, the dependence becomes stronger. For currents less than 100 a, the dependence is so weak that it seems to vanish. Lengthening the gap seems to cause the current to decrease for a given source conductance. Thus, even though the source conductance is the major factor

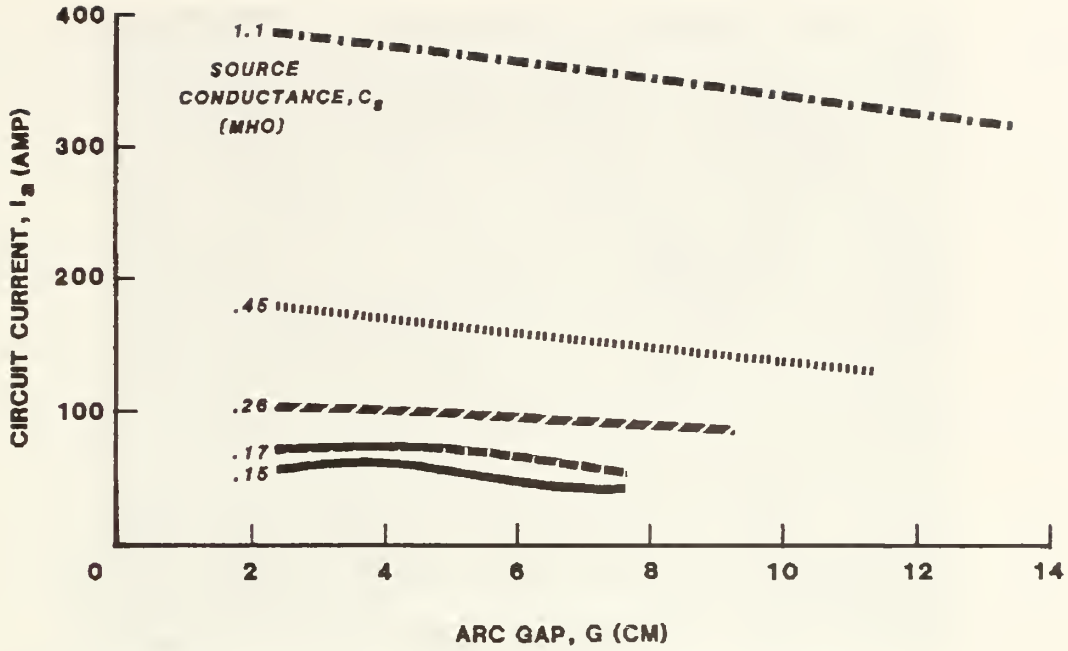

Figure 16—Circuit current as a function of arc gap for four values of source conductance.

determining the current flow, the arc length does have an effect. This still does not mean that the current and the voltage drop are significantly related. Before expanding further on the current and voltage drop of the arc, we need to look at the details of arc behavior with time.

RESULTS OF EXPERIMENTS—DETAILED ARC TIME BEHAVIOR

From consideration of the overall arc parameters, we turn to the details of the time behavior. A typical arc cycle was presented in figure 2. The current trace displays the initial pulse (1), followed by a drop in current for about 200 to 300 μs (2), then a current rise (3), a noisy period followed by a quiet high-current flow (4), and the turn-off pulse (5). We will consider these phases of the total arc duration separately.

Figure 17 is a single frame from a 1,000 frame/s video system. The 0.1-mm-diameter tungsten wire is heated by the circuit current. In the appendix, a simple analysis predicts a duration of about 135 μs. The appendix calculation does not take into account the radiative losses as the wire heats, which would make the time somewhat longer. Figure 18 presents current in the wire and light output as a function of time for the wire heating phase of the arc. The current trace has a high initial peak, as we saw in the shorted case of figure 7. This represents charging of the SCR capacitance. The actual turn-on time of the SCR is reflected in the slow rise, peaking at about 35 μs from initiation. At this point, the wire begins to heat, as can be seen from the light output trace. The heating time can be seen on the trace as somewhat longer than the 135 μs as calculated. The events labeled B and C on figure 18 are present on all the traces we have looked at in this detail, but in the absence of detailed photography, we do not know what phenomenon causes them. Event C may well be the creation of a local hot spot and the beginning of the disintegration of the wire. There is no corresponding variation in the current, but the presence of a local small break would not necessarily cause a noticeable change in current flow. The same events for a different arc are evident in figure 19. Here, event B occurs later than in the example of figure 18. The former figure illustrates the connection of event B to the wire separation or perhaps to the beginnings of the formation of the arc, corresponding to the period calculated in the appendix. The current rise subsequent to event B is from the arc-striking process.

Subsequent to the wire heating and breaking or disintegrating, the arc strikes in the ionized column left behind. A time history of this part of the arc duration is shown by figures 20 and 21. Here, the wire heating phase is short and not well-defined. Voltage instead of light output was recorded for this event (there are only two channels in the recording oscilloscope). In figure 20a, the anode can be seen under the "E" in "Ektapro" and the cathode is just out of the picture between the "A" and "Y" of "PLAY." Refer to figure 10 again for the physical layout. In figure 20a, the wire has disintegrated, leaving behind remnants of burning tungsten, seen as the bright dots in the figure, a-f. The anode and cathode jets have begun to form, can just be seen in figure 20a, and are apparent in figures 20c-20f. The time elapsed between figures 20a and 20f is 13 ms.

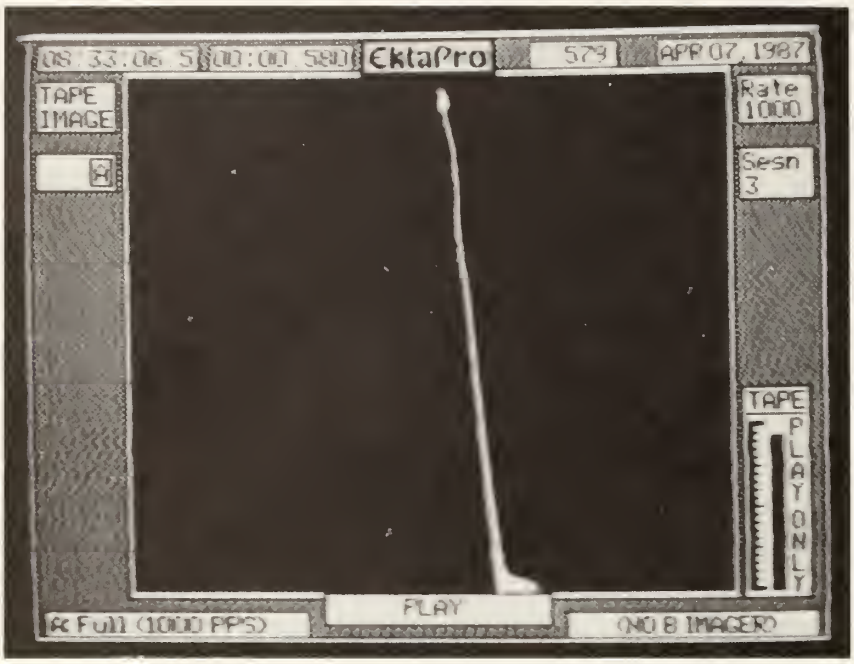

Figure 17—A frame of fast video recording of the wire heating part of arc formation.

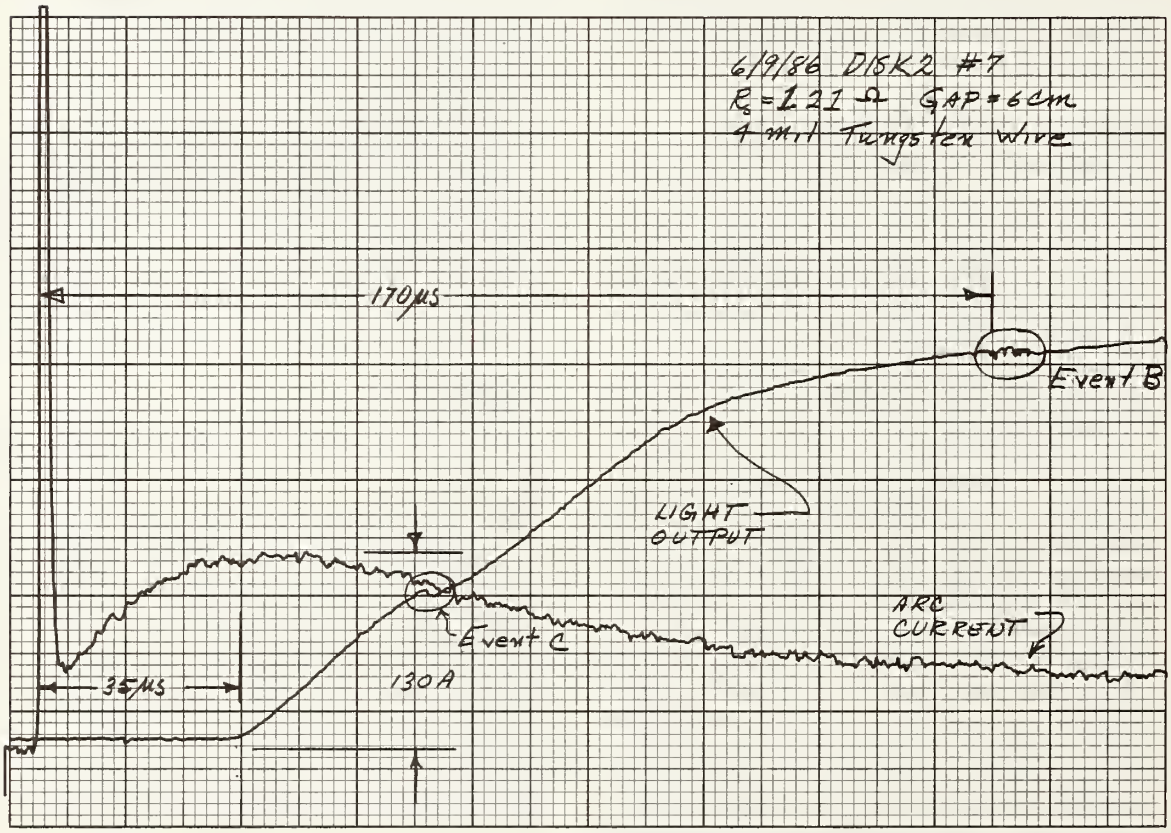

Figure 18—A high time resolution record of circuit current and arc luminosity for the wire heating part of arc formation.

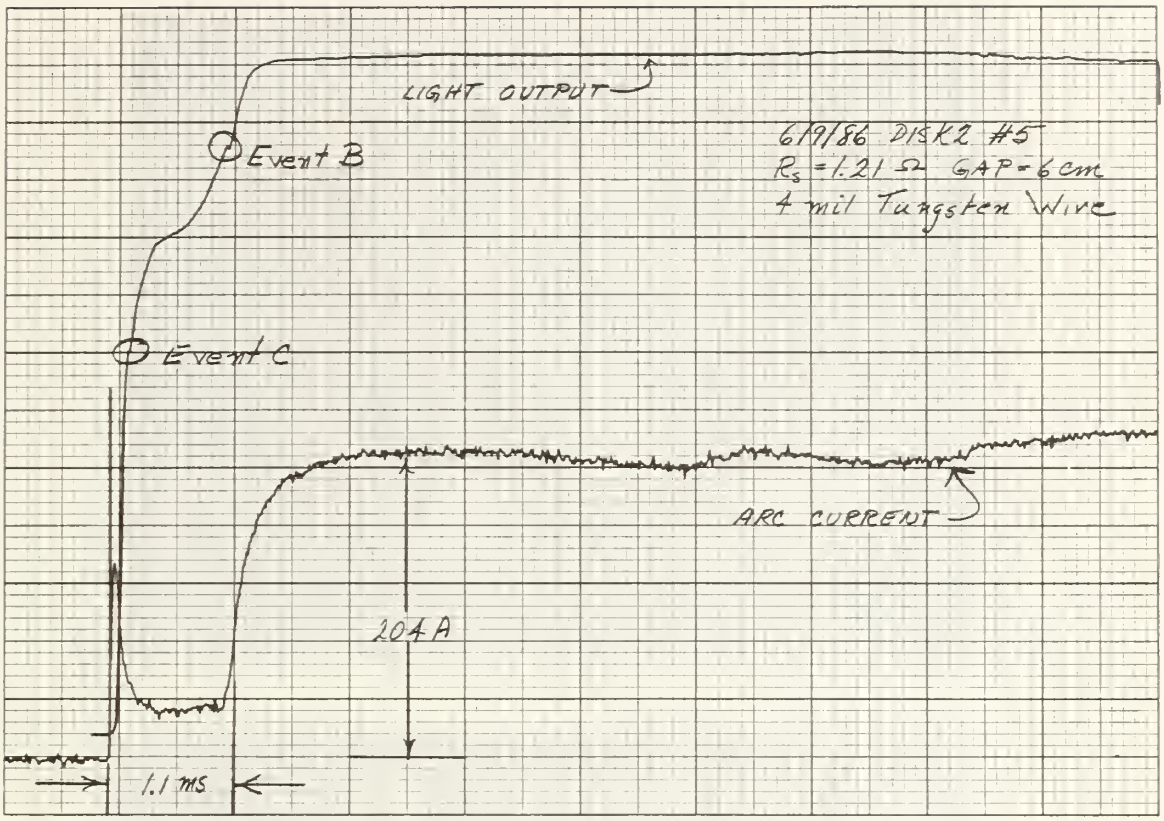

Figure 19—A medium resolution record of wire heating and arc striking parts of arc formation.

a

Figure 20—Successive frames (a-f) from a fast video recording of the formation part of an arc discharge.

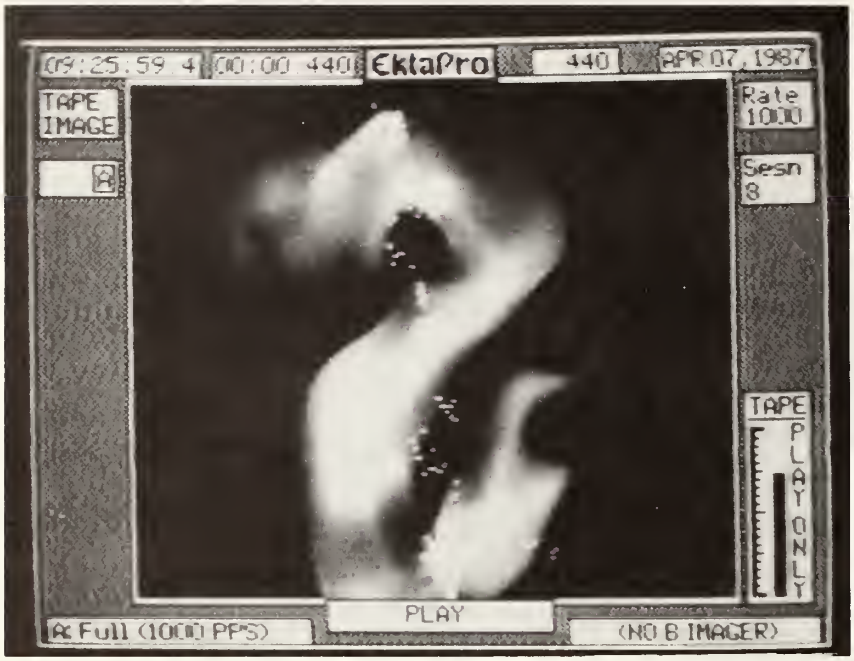

b

c

Figure 20 (Con.)

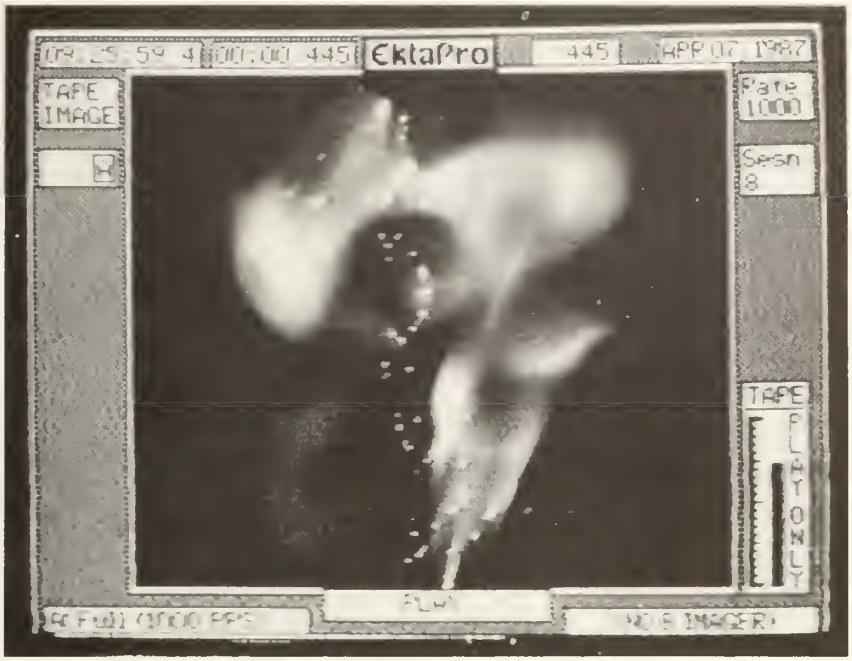

d

e

Figure 20 (Con.)

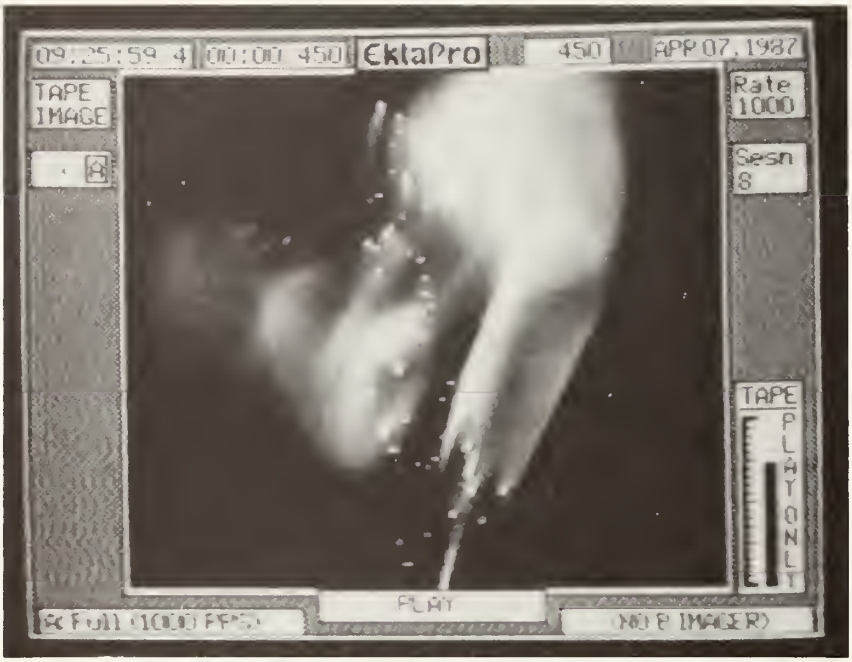

f

Figure 20 (Con.)

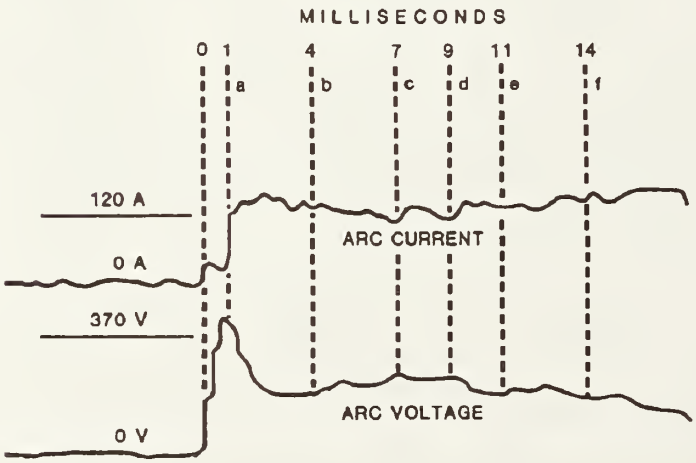

Figure 21—The current and voltage record accompanying figure 20. Note the keys to that figure.

We have correlated the images of figure 20 to the current and voltage traces of figure 21. Initial current and voltage spikes are missing and the voltage trace is ragged at the onset (between 0 and 1 ms) because the time scale was expanded for this measurement; there are five sample values between these points. Despite the violent and transitory nature of the hot gases in the arc, the current and voltage traces seem rather quiet; they do reflect the changes in the arc gas structure, but the variations are about 10 to 15 percent of the peak value. In general, the more tenuous and torturous the path, the lower the current, as for example at c and d of figures 20 and 21. As the path shortens, and the image brightens, the current increases, as at f (figs. 20 and 21). This behavior is consistent with the known characteristics of hot air conductivity as a function of temperature. Between 4,500 K and 10,000 K, the conductivity of air is very nearly constant. This means that even though the brightness of the arc as seen by the video camera might vary significantly, the conductance of the arc will not vary by much. Length changes, on the other hand, will have a direct effect on arc conductance, with the current decreasing as the arc length increases. In this case, the voltage is affected as well.

The voltage at the time the arc strikes (point a, figure 21) was called the striking voltage. Although the voltage displayed is less than the true voltage because of the time lag in the voltmeter, it is nonetheless instructive to consider how striking voltage varies with arc gap and source conductance. This is done in table 5 and figure 22. The analysis presented in the table indicates that the conductance has little to do with the striking voltage. This means that the breakdown of the path depends only on the voltage across the gap in the ionized medium for the conductance values attainable with this apparatus. The electric field at the time of striking the arc is, from figure 22, about 37 V/cm, again probably lower than the true value. Apparently, there is a problem with maintaining the arc for gaps greater than 10 cm. The voltage drop at striking would be on the order of 400 V by measurement.

Table 5—Linear regression analysis for arc striking voltage as a function of gap and source conductance for the side-strike method

	Unweighted least squares linear regression of voltage			
Predictor variables	**Coefficient**	**Std error**	**Student's T**	**P**
Constant	104.71	9.7674	10.72	0.0000
Cond	−21.116	12.493	−1.69	.1021
Gap	34.851	1.6391	21.26	.0000

Cases included	31	Missing cases	4
Degrees of freedom	28		
Overall F	284.1	P value	0.0000
Adjusted R^2	.9497		
R^2	.9530		
Resid. mean square	469.5		

	Stepwise analysis of variance of voltage						
Source	**Individual SS**	**Cum. DF**	**Cumulative SS**	**Cumulative MS**	**Adjusted R^2**	**Mallow' CP**	**P**
Constant	3.1215E+06						
Cond	5.4509E+04	1	5.4509E+04	5.4509E+04	0.1670	453.1	2
Gap	2.1224E+05	2	2.6675E+05	1.3337E+05	.9497	3.0	3
Residual	1.3146E+04	30	2.7989E+05	9329.8			

Cases included	31	Missing cases	4
Degrees of freedom	28		
Overall F	284.1	P value	0.0000
Adjusted R^2	.9497		
R^2	.9530		
Resid. mean square	469.5		

	Unweighted least squares linear regression of voltage			
Predictor variables	**Coefficient**	**Std error**	**Student's T**	**P**
Constant	104.37	10.073	10.36	0.0000
Gap	33.427	1.4502	23.05	.0000

Cases included	31	Missing cases	4
Degrees of freedom	29		
Overall F	531.3	P value	0.0000
Adjusted R^2	.9465		
R^2	.9482		
Resid. mean square	499.5		

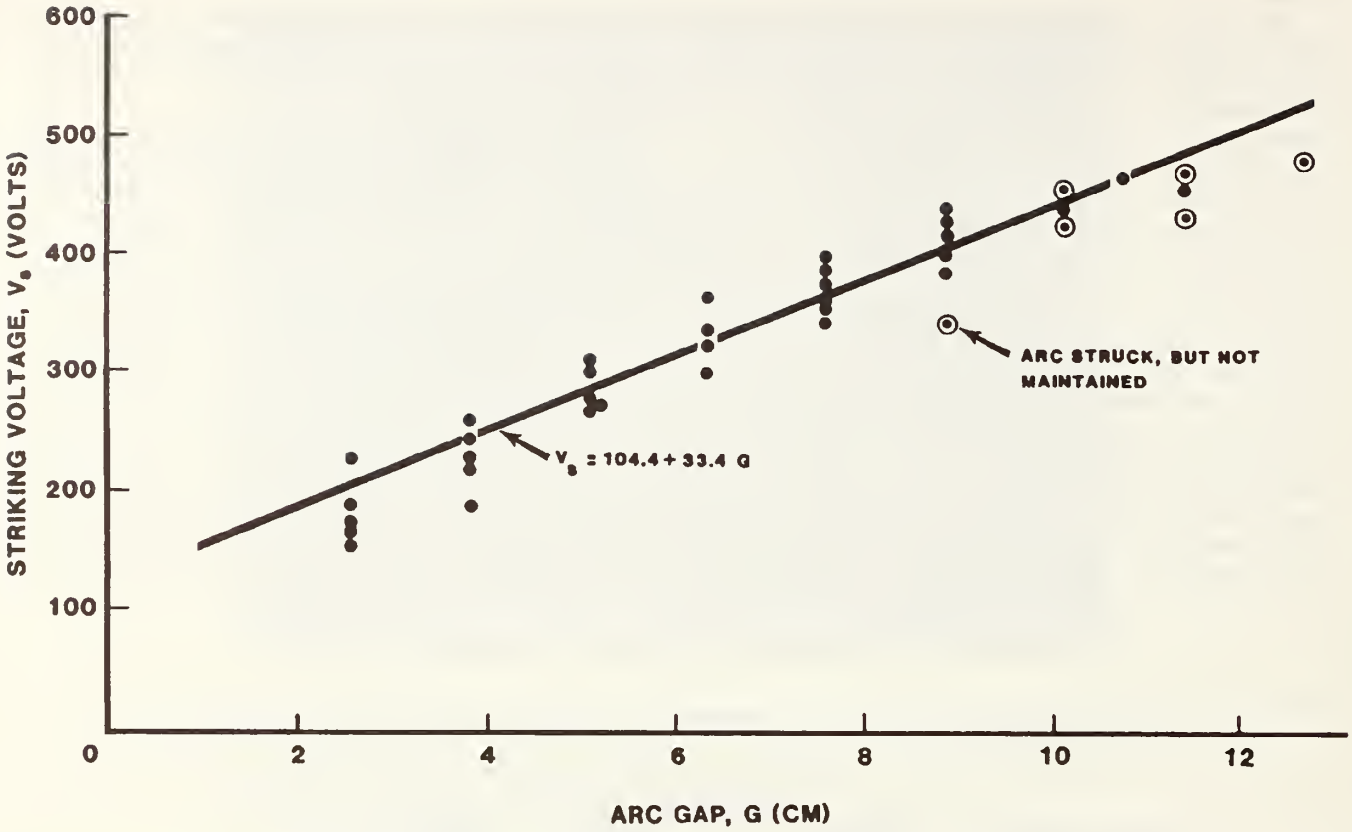

Figure 22—The voltage drop across the arc as it strikes as a function of arc gap.

The current at striking is on the order of 10 A, and the voltage drop in the external circuit is about 100 V. The small effect which might be present due to the source conductance is masked by experimental noise.

The striking mechanism was examined by Vlastos (1973). Although the voltages in his exploding wire experiments were higher than ours by more than a factor of 2, the mechanism he gives for "low" voltage sources is, from the fast video evidence, the one at work in our study. The wire heats slowly, relative to heating rates for 10 kV sources, and no shock wave forms from the rapid heating. Because there is no shock wave, and the wire heats slowly, there is an ion cloud formed around the wire, and it is in this medium that the arc forms. This is clear from figure 20a and b, where the hot gas cloud containing the discharge has moved away from the remains of the wire, seen as hot spots between the cathode and the anode. The column of gas has moved away because of buoyancy and the electromagnetic forces. Note that the separation of the trigger wire may be event c in figure 19. This is suggested by the presence of a "dwell time" in Vlastos' data; a time between wire breaking and arc formation. The dwell time in our data seems to be on the order of 1 ms, 20 times Vlastos' longest dwell time. This is expected from the lower voltage available in our apparatus, as an extrapolation of his data indicates.

Striking of the arc with the "pull-down" pneumatic cylinder apparatus is quite different, as can be seen from figures 23 and 24. Here, the arc forms as the cathode travels away from the anode. The cathode jet is always well formed, but its extension rate may or may not be sufficient to keep up with the withdrawal rate of the cathode. The voltage and current traces show the gradual decrease of current as the arc lengthens and settles into a steady state. There is a 33-ms delay between the current turn-on pulse and the beginning of the cathode motion because of computer timing delay. The actual motion of the cathode starts after this delay, and proceeds for about 60 ms (figs. 23, 24). Note that there seems to be a "second strike" in the case shown in figure 24. Because we do not have high-speed visual data, we cannot yet say what the cause is for this behavior. It may be that the formation of the cathode and anode jets simply cannot proceed as fast as the cathode is withdrawn in some cases.

The arc does not deviate to one side as much as in the wire experiments because we have moved the anode supply wire so that it is on the arc axis rather than perpendicular to it. The trace after the cathode has reached full extension is very well behaved by comparison with the exploding wire experiments. Details of the pulled arc are not yet available.

The effect of hydrodynamic instability and the perpendicular lead is apparent from the behavior of the arc subsequent to striking, as shown in figures 25, 26, and 27. Figure 27 is the fast video, and is about one cycle of the current and angle traces of figure 26. The video data

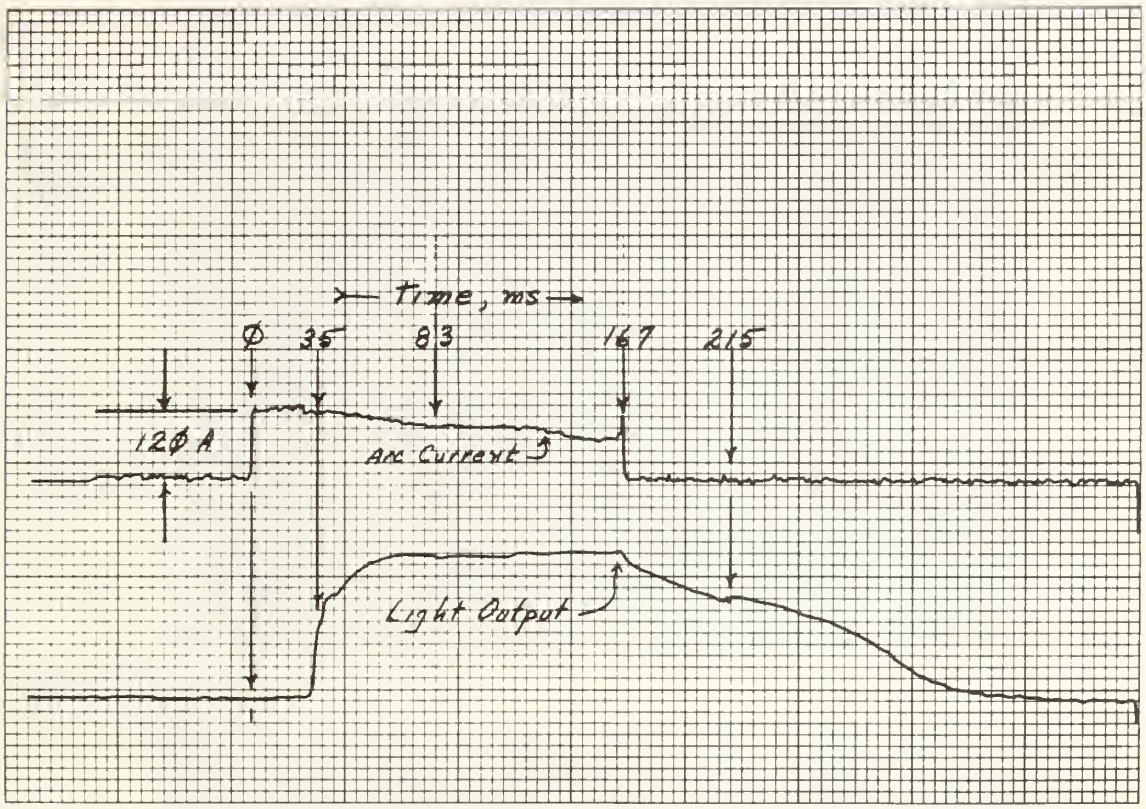

Figure 23—Arc current and luminosity records for "pull-down" ignition.

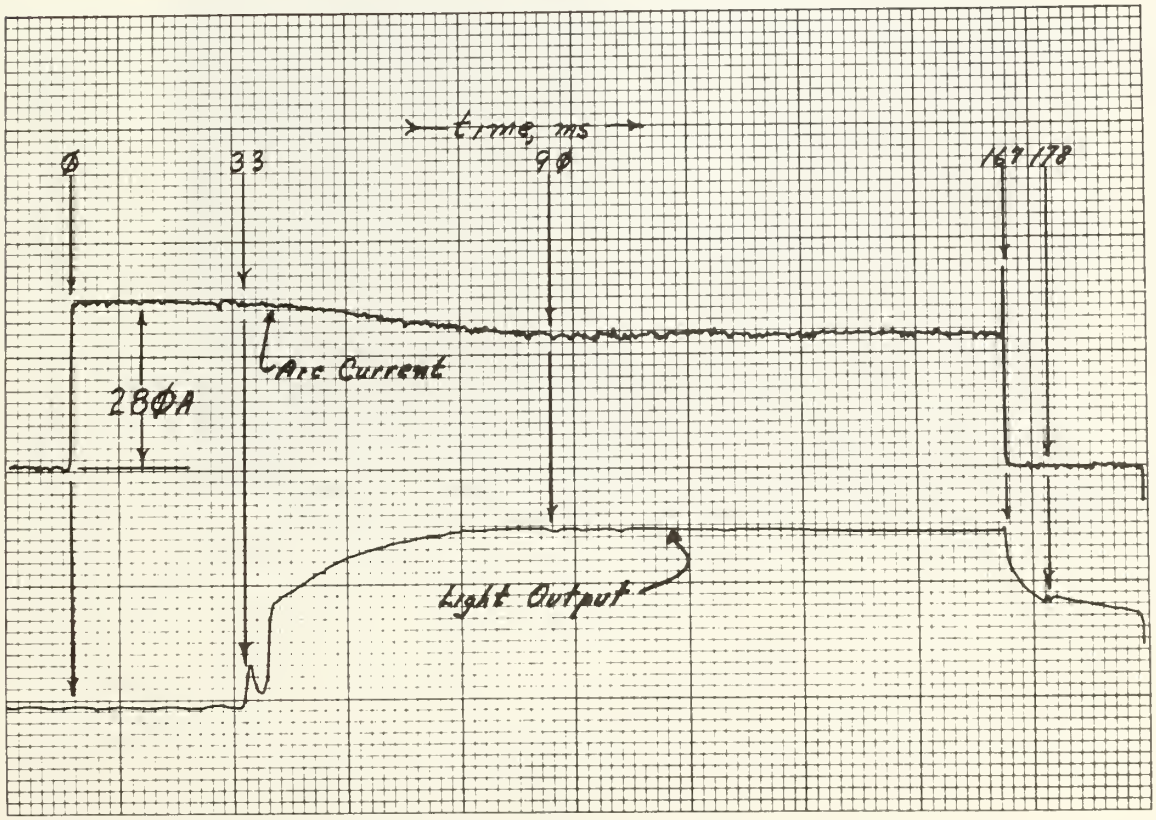

Figure 24—As figure 23, showing a second strike.

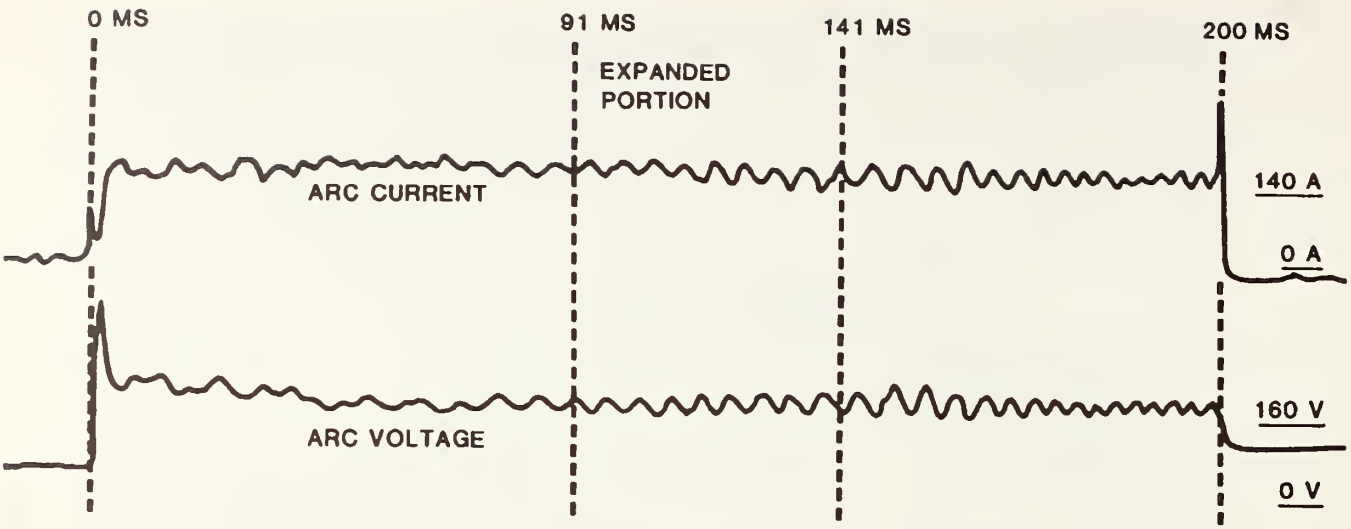

Figure 25—Current and voltage records for an oscillating arc.

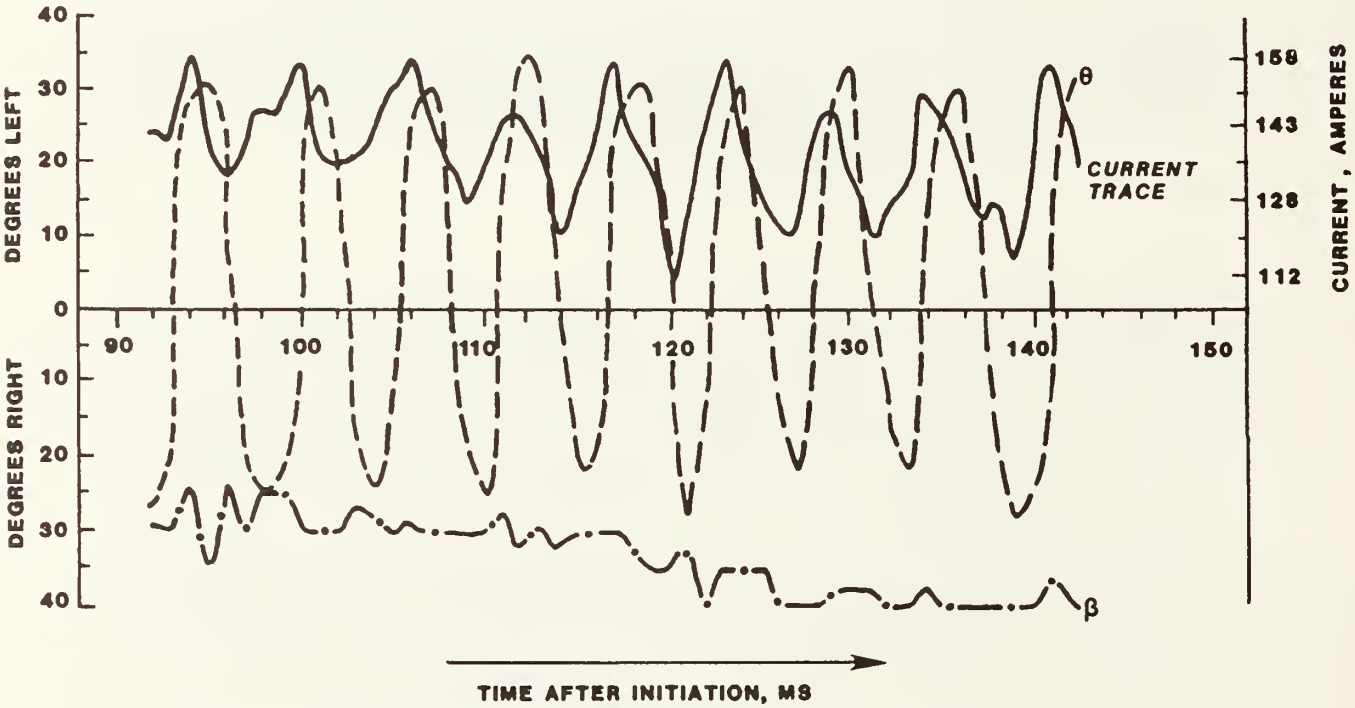

Figure 26—The expanded portion of figure 25, with the apparent angles to the vertical of the anode jet (theta) and cathode jet (beta). The angles were measured from the video records shown in figure 27.

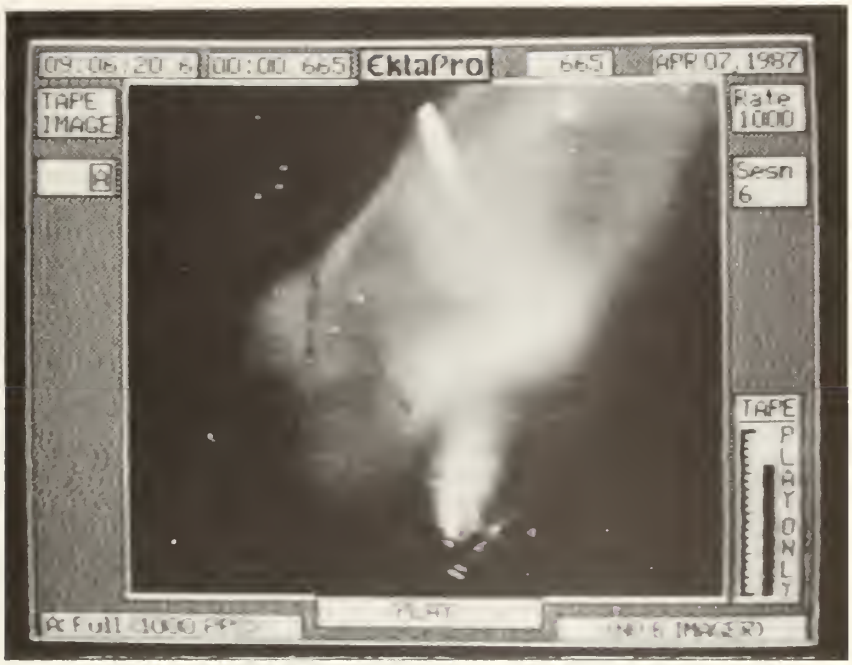

a

b

Figure 27—Successive video frames (a-j) of oscillatory arc behavior.

c

d

Figure 27 (Con.)

e

f

Figure 27 (Con.)

g

h

Figure 27 (Con.)

i

j

Figure 27 (Con.)

clearly show oscillation of the arc anode jet, very likely rotation (an impression from watching the video) about the relatively stable cathode jet. Figure 26 is a time history of the angle of the jets together with the current in the arc. It corresponds to the time period in figure 25 labeled "expanded portion." The jet angle is taken from the video by protractor with respect to the anode-cathode axis. Although anode jet regions are not usually a feature of vertical arcs, they have been observed (Lutz and Pietsch 1980), and look very much like those shown here. Note (Maecker 1971) that the current carrying portion of the arc does not always coincide with the brightest part of the video record, particularly in the diffuse area connecting the cathode and anode jets.

The angular positions of the anode (theta) and cathode (beta) jets with respect to the vertical are shown in figure 26. During this 50 ms of the arc, the anode undergoes about nine oscillations, or a period of about 5.2 ms. Because there is a fuel sample present at the cathode in this arc, the cathode region is seen by the camera to be diffuse. Processing to obtain figures for publication enhances the fuzziness, so that the cathode jet is hidden. In the original videotape the cathode jet is apparent and can be measured. (An unobscured jet can be seen in figure 29a.)

The current trace is also shown on figure 26. Surprisingly, the current is near minimum when the anode jet appears to be closest to the cathode jet, opposite to the condition that might be expected. This is probably an artifact of the two-dimensional view. There is an apparent phase shift as well, perhaps due to the same cause. The current oscillations in this case are about 15 percent of the mean current, as can be seen in figures 25 and 26. Although current records from other arcs show less organized variations in the current, and sometimes greater, the cause of the variations is undoubtedly anode jet wander. High-speed videos of three other arcs, taken on the same day as those of figure 27, verify this view.

We chose one of the other arcs to display the characteristics of the end of the arc time. Figure 28 is the current and light output of a short arc meant to display "shutdown," and figure 29 fast video frames from another arc. Again, we did this to show the light output behavior instead of voltage.

In figure 29, the shutoff of the SCR switch can be clearly seen on the current trace at the end of the 45-ms arc. A large spike is present in all records at shutoff due to commutation of the switch SCR. At shutoff, current flow ceases cleanly, and the gas begins to cool quickly as predicted (Latham 1986). Cooling is also seen in video frames figure 29 b,c,d. Because the arc of figure 29 had no fuel sample present at the cathode, the cathode jet is clearly visible without a haze due to burning material. Note that figure 29a is about 200 ms prior to the remaining frames, which are 1 ms apart and indicate the rapid decay of the hot gas temperature after the current is interrupted.

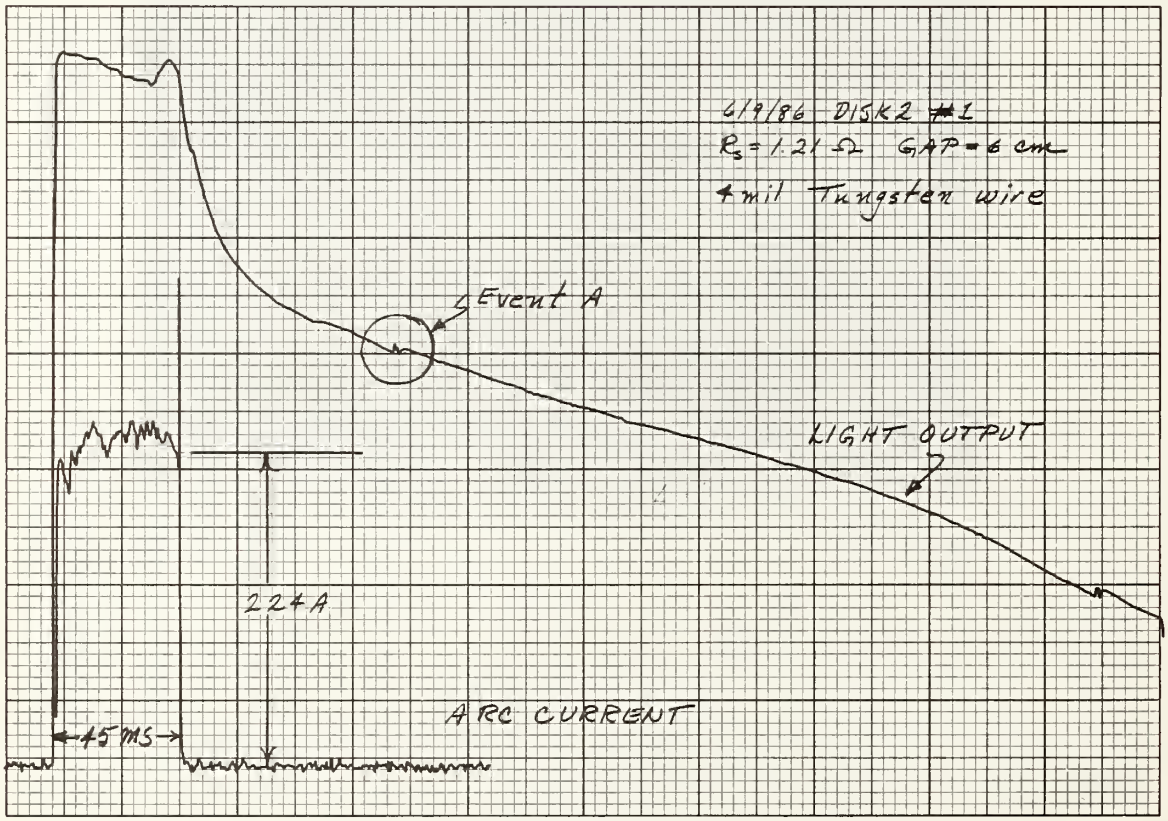

Figure 28—Current and light output records showing arc shut-off.

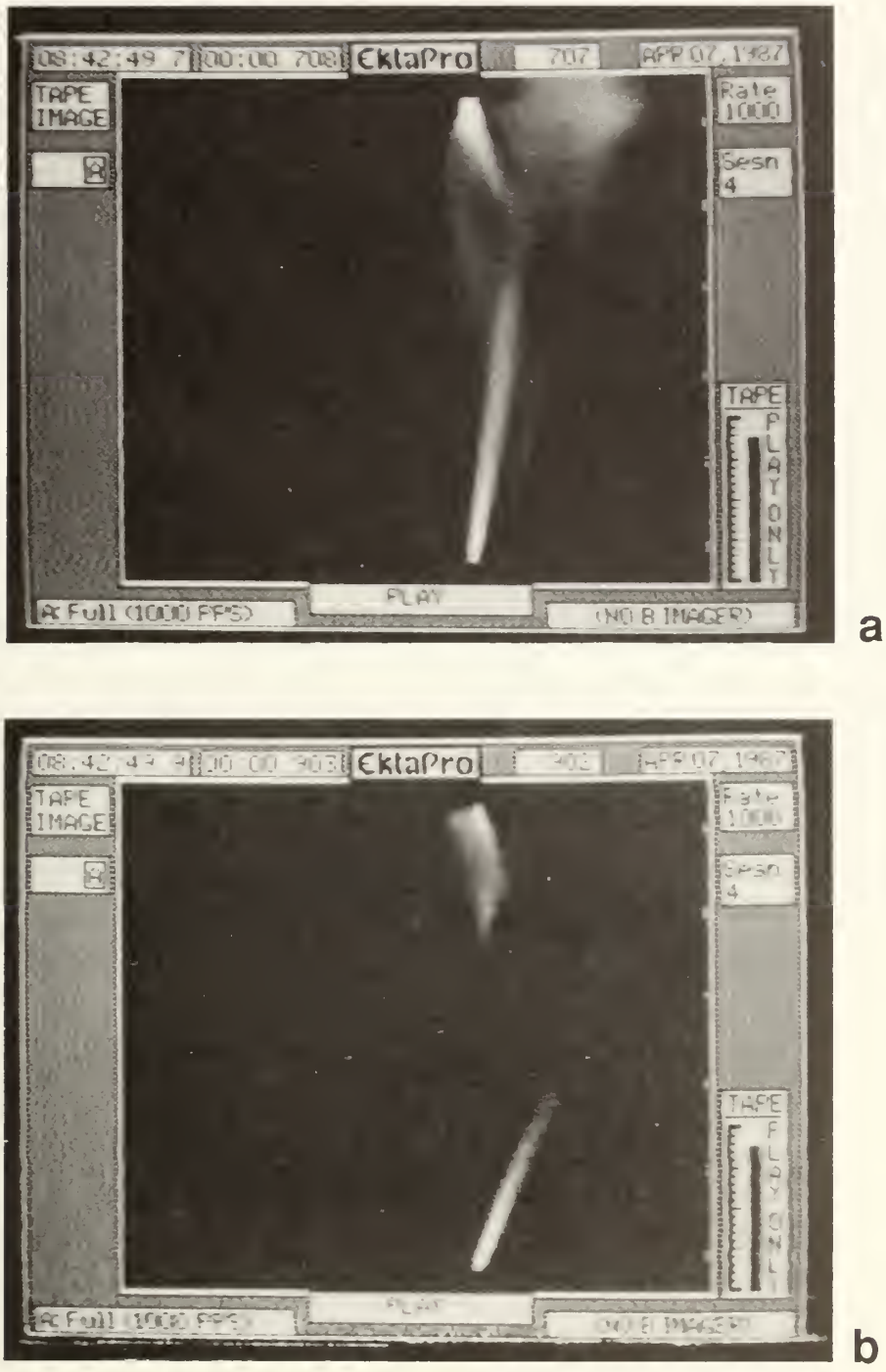

Figure 29—A well-formed typical arc; b,c,d: fast video of the shut-off of the same arc.

c

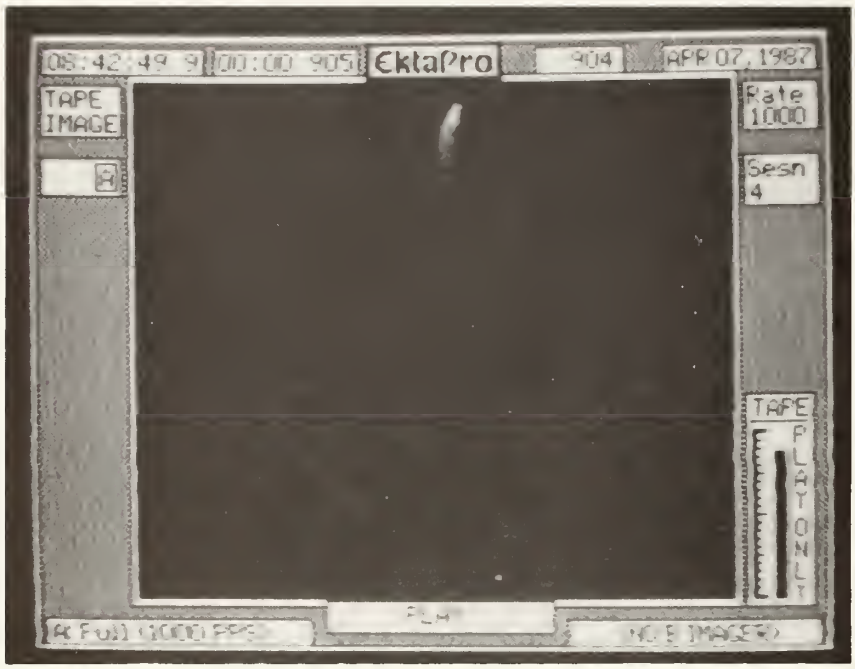

d

Figure 29 (Con.)

The light decay curve, figure 28, has a small variation, labeled Event A. This event occurred in every case looked at with the light sensor. There was no corresponding event in either the voltage or the current. Further, the event was not a constant time after the shutoff pulse, although it seemed to happen at about the same place on the decay curve. We do not know whether this is an electrical artifact, or an event occurring over a very narrow temperature range of the cooling gas, causing a change in emission. An optical spectrometer might provide more information about this event.

SUMMARY AND CONCLUSIONS

The arc behavior has now been described in both gross terms and in time detail. There are many questions raised by even the relatively little fast video data. Due to limitations of time and instrumentation, we will probably not be able to continue the investigation. Nevertheless, we have found that free arcs of the length and current range used in this study have the following characteristics:

- a stable, nearly cylindrical, cathode jet
- a wandering anode jet
- voltage drop dependent only on electrode gap
- current flow dependent only on the electrical source
- gross electrical and cathode jet stability despite flow instabilities
- sufficient predictability and reliability for ignition studies.

REFERENCES

King, L. A. 1961. The voltage gradient of the free-burning arc in air or nitrogen. ERA Report G/XT172. Leatherhead, Surrey: The British Electrical and Allied Industries Research Association. 14 p.

Latham, D. J. 1980. A channel model for long arcs in air. The Physics of Fluids. 23(8): 1710-1715.

Latham, D. J. 1986. Anode behavior of long vertical air arcs at atmospheric pressure. IEEE Transactions on Plasma Science. PS-14(3): 220-227.

Latham, D. J. 1987. Design and construction of an electric arc generator for fuel ignition studies. Res. Note INT-366. Ogden, UT: U.S. Department of Agriculture, Forest Service, Intermountain Research Station. 15 p.

Lutz, F.; Pietsch, G. 1980. Investigation of the pressure rise in the surroundings of a high-current fault arc. In: Gas discharges and their applications. IEEE Conf. Publ. 189. Riccarton, Edinburgh, UK: Heriot-Watt University: 270-273.

Maecker, H. H. 1971. Principles of arc motion and displacement. Proceedings of the IEEE. 59(4): 439-449.

Somerville, J. M. 1959. The electric arc. New York: John Wiley & Sons. 150 p.

Strachan, D. C.; Barrault, M. R. 1975. Axial velocities in the high current free burning arc. Report ULAP-T34. Liverpool, UK: University of Liverpool, Department of Electrical Engineering and Electronics. 10 p.

Strom, A. P. 1946. Long 60-cycle arcs in air. AIEE Transactions. 65: 113-117.

Vlastos, A. E. 1973. Dwell times of thin exploding wires. Journal of Applied Physics. 44(5): 2193-2196

von Engel, A. 1965. Ionized gases. Oxford: Clarendon Press. 289 p.

APPENDIX

To do the exploding wire problem in a simple form
using the equivalent circuit of a battery in series
with a current-limiting resistance and the wire.
Assume that all Joule heating stays in the wire.

Battery voltage	V := 500	volts
series resistance	Rs := 1.21	ohms
wire diameter	Dia := .01	cm
wire length	Len := 6	cm
melting point Tungsten	Tf := 3400	deg. C
ambient temperature	To := 20	"

Wire volume

$$vol := \pi \cdot Len \cdot \left[\frac{Dia}{2}\right]^2 \qquad vol = 4.712 \cdot 10^{-4}$$

Wire density rho := 19.3 g/cm^3

Functions:
Specific heat and resistivity of Tungsten:

$$Cp(T) := .13 + 17.2 \cdot 10^{-6} \cdot T \quad \text{joule/g-degC}$$

$$Res(T) := 5.53 \cdot 10^{-6} \cdot (1 + .0045 \cdot T) \quad \text{ohm-cm}$$

The resistance of the wire is thus:

$$Rw(T) := Res(T) \cdot \frac{Len^2}{vol} \quad \text{ohms,}$$

the current flow in the circuit is:

$$I(T) := \frac{V}{Rs + Rw(T)}$$, and the power is: $P(T) := I(T)^2 \cdot Rw(T)$

So, if t is the time taken to reach the melting point of the wire,

$$t(Tf) := \int_{To}^{Tf} rho \cdot vol \cdot \frac{Cp(T)}{P(T)}\, dT \qquad \tau(Tf) := t(Tf) \cdot 10^6$$

For this example, then, $\tau(Tf) = 135.327$ μsec

To get the time behavior, set index k := 1 ..170

and define a set of temperatures, $Tv_k := 20 \cdot k$

then if $tim_k := \tau\left[Tv_k\right]$,

and if $cur_k := I\left[Tv_k\right]$,

the following time behavior is obtained:

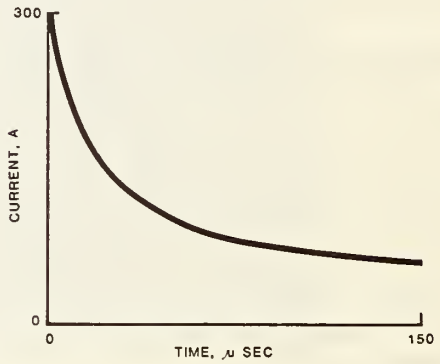

Latham, Don J. 1989. Characteristics of long vertical DC arc discharges. Res. Pap. INT-407. Ogden, UT: U.S. Department of Agriculture, Forest Service, Intermountain Research Station. 32 p.

Experiments were conducted to ascertain the discharge characteristics of direct-current arcs approximately 10 cm in length, in an effort to estimate the fire-starting potential of lightning and downed powerlines. Vertical arcs of this length were generated by a high-current battery and an SCR switching system. Voltage-current relationships depend on arc length and source conductance. Voltage drop across the arc depends largely on arc length and is independent of the current. Current flow is independent of length, but dependent on source conductance. Arc behavior generally agrees with an earlier theoretical model. High-speed video images of arcs are included in this report.

KEYWORDS: electrical physics, ignition, electrical discharges, lightning

INTERMOUNTAIN RESEARCH STATION

The Intermountain Research Station provides scientific knowledge and technology to improve management, protection, and use of the forests and rangelands of the Intermountain West. Research is designed to meet the needs of National Forest managers, Federal and State agencies, industry, academic institutions, public and private organizations, and individuals. Results of research are made available through publications, symposia, workshops, training sessions, and personal contacts.

The Intermountain Research Station territory includes Montana, Idaho, Utah, Nevada, and western Wyoming. Eighty-five percent of the lands in the Station area, about 231 million acres, are classified as forest or rangeland. They include grasslands, deserts, shrublands, alpine areas, and forests. They provide fiber for forest industries, minerals and fossil fuels for energy and industrial development, water for domestic and industrial consumption, forage for livestock and wildlife, and recreation opportunities for millions of visitors.

Several Station units conduct research in additional western States, or have missions that are national or international in scope.

Station laboratories are located in:

Boise, Idaho

Bozeman, Montana (in cooperation with Montana State University)

Logan, Utah (in cooperation with Utah State University)

Missoula, Montana (in cooperation with the University of Montana)

Moscow, Idaho (in cooperation with the University of Idaho)

Ogden, Utah

Provo, Utah (in cooperation with Brigham Young University)

Reno, Nevada (in cooperation with the University of Nevada)